Ubiquitin ligases and a processive proteasome facilitate protein clearance during the oocyte-to-embryo transition in *Caenorhabditis elegans*

Caroline A. Spike*, Tatsuya Tsukamoto*, and David Greenstein*,[1]

*Department of Genetics, Cell Biology and Development, University of Minnesota, Minneapolis, Minnesota 55455, USA

9 Running title: Protein Degradation During the OET

10

11 Keywords: oocyte meiotic maturation, oocyte-to-embryo transition, translational regulation,

12 RNA-binding proteins, ubiquitin-mediated protein degradation

13

14 [1]Corresponding author: David Greenstein, Department of Genetics, Cell Biology, and

15 Development, University of Minnesota, 4-208 MCB, 420 Washington Avenue SE, Minneapolis,

16 MN 55455. Tel: 612-624-3955; FAX: 612-626-6140. E-mail: green959@umn.edu

17

ABSTRACT

The ubiquitin-mediated degradation of oocyte translational regulatory proteins is a conserved feature of the oocyte-to-embryo transition (OET). In the nematode *Caenorhabditis elegans*, multiple translational regulatory proteins, including the TRIM-NHL RNA-binding protein LIN-41/Trim71 and the Pumilio-family RNA-binding proteins PUF-3 and PUF-11, are degraded during the OET. Degradation of each protein requires activation of the M-phase cyclin-dependent kinase CDK-1, is largely complete by the end of the first meiotic division and does not require the anaphase promoting complex (APC). However, only LIN-41 degradation requires the F-box protein SEL-10/FBW7/Cdc4p, the substrate recognition subunit of an SCF-type E3 ubiquitin ligase. This finding suggests that PUF-3 and PUF-11, which localize to LIN-41-containing ribonucleoprotein particles (RNPs), are independently degraded through the action of other factors and that the oocyte RNPs are disassembled in a concerted fashion during the OET. We develop and test the hypothesis that PUF-3 and PUF-11 are targeted for degradation by the proteasome-associated HECT-type ubiquitin ligase ETC-1/UBE3C/Hul5, which is broadly expressed in *C. elegans*. We find that several GFP-tagged fusion proteins that are degraded during the OET, including fusions with PUF-3, PUF-11, LIN-41, IFY-1/Securin and CYB-1/Cyclin B, are incompletely degraded when ETC-1 function is compromised. However, it is the fused GFP moiety that appears to be the critical determinant of this proteolysis defect. These findings are consistent with a conserved role for ETC-1 in promoting proteasome processivity and suggest that proteasomal processivity is an important element of the OET during which many key oocyte regulatory proteins are rapidly targeted for degradation.

Article Summary

The ubiquitin-mediated degradation of translational regulatory RNA-binding proteins is a conserved feature of the oocyte-to-embryo transition (OET). *C. elegans* LIN-41 is a master regulator of oogenesis and is found in a large translational regulatory ribonucleoprotein (RNP) complex with more than 1000 maternal transcripts and the Pumilio-family RNA-binding proteins PUF-3 and PUF-11. We show that the concerted action of ubiquitin-mediated protein degradation and proteasome processivity rapidly disassemble LIN-41-containing RNPs during the OET thereby relieving repression of many maternal transcripts.

INTRODUCTION

The oocyte-to-embryo transition (OET) initiates when oocytes exit meiotic prophase and enter the first meiotic metaphase, a cell cycle and developmental event also known as meiotic resumption or meiotic maturation. The OET is complete when zygotic gene transcription begins after fertilization in the early embryo. In many mammals and in the nematode *Caenorhabditis elegans*, zygotic gene transcription begins early at the 2- or ~4-cell stage, respectively (Clegg and Pikó 1982; Latham *et al*. 1991; Edgar *et al*., 1994; Seydoux and Fire 1994; Hamatani *et al*. 2004). In some animals, such as Drosophila and Xenopus, zygotic gene activation predominantly begins later—at approximately the eighth nuclear division in Drosophila (Pritchard and Schubiger 1996; reviewed by Harrison and Eisen 2015) and at the midblastula transition in Xenopus (Bachvarova *et al.* 1966; Newport and Kirschner 1982a,b; reviewed by Blitz and Cho 2021). Because the late-stage oocytes of most animals are transcriptionally quiescent, the regulation of protein translation by RNA-binding proteins represents a dominant mode of developmental control during oocyte meiotic maturation and the OET (reviewed by Kotani *et al*. 2017; Huelgas-Morales and Greenstein 2018; Teixeira and Lehmann 2019). In fact, genomic analyses suggest that mammalian oocytes contain more than 200 RNA-binding proteins (Luong and Conti 2019). The presumption is that many of these RNA-binding proteins regulate protein translation in oocytes and preserve the dowry of maternal mRNA contributed to the early embryo.

In *C. elegans* oocytes, the TRIM-NHL RNA-binding protein LIN-41 is a key component of a large translational regulatory RNP complex that associates with more than 1000 mRNAs (Spike *et al*. 2014b; Tsukamoto *et al*. 2017). Many of these mRNAs encode protein components of LIN-41-containing RNPs and function as translational regulators during oogenesis or early

72 embryonic development. LIN-41 also mediates the 3'-untranslated region (UTR)-mediated
73 translational repression of some of the transcripts that associate with LIN-41 in oocytes and has
74 an essential function to promote the extended meiotic prophase of oocytes (Spike *et al*. 2014a,b;
75 Tsukamoto *et al*. 2017). *lin-41* null mutants are sterile because they produce pachytene-stage
76 oocytes that exit meiotic prophase prematurely; these oocytes inappropriately disassemble the
77 synaptonemal complex, cellularize, activate the CDK-1/cyclin B cyclin-dependent kinase, and
78 enter M phase (Spike *et al*. 2014a). Hypomorphic *lin-41* mutant alleles reduce oocyte quality and
79 cause nondisjunction during female meiosis (Spike *et al*. 2014a). LIN-41 prevents the premature
80 activation of the CDK-1/cyclin B during early oogenesis, in part, through the 3'UTR-mediated
81 translational repression of the CDC-25.3 phosphatase, a CDK-1 activator (Spike *et al*. 2014a,b).
82 Premature CDK-1 activation in *lin-41* mutant oocytes drives precocious M-phase entry and
83 causes oocytes to abnormally transcribe and express genes that are normally expressed
84 zygotically after the OET (Allen *et al*. 2014; Spike *et al*. 2014a; Tocchini *et al*. 2014; Matsuura
85 *et al.* 2016). Thus, a major function of LIN-41 appears to be to preserve mRNAs that are
86 maternally inherited and translationally activated late in oogenesis or during early embryonic
87 development. Many LIN-41-associated transcripts are translated only after LIN-41 is inactivated
88 and degraded via ubiquitin-mediated degradation upon the onset of meiotic maturation (Spike *et*
89 *al*. 2018). For example, LIN-41 associates with and represses the translation of the ORC-1
90 subunit of the origin recognition complex during meiotic prophase, and its degradation permits
91 ORC-1 expression for DNA replication in the embryo (Tsukamoto *et al*. 2017).

92 LIN-41 is highly conserved and its mammalian ortholog, LIN-41/TRIM71, is required for
93 embryonic viability and neural tube closure in mice (Maller Schulman *et al*. 2008; Chen *et al*.
94 2012; Cuevas *et al*. 2015; Mitschka *et al*. 2015). This defect appears to be related to a

95 requirement for LIN-41/TRIM71 for maintaining pluripotency in neural progenitor cells in the
96 embryo. LIN-41/TRIM71 has also been found to promote the pluripotency of embryonic stem
97 cells in the mouse (Chang *et al*. 2012; Worringer *et al*. 2014; Mitschka *et al*. 2015; Liu *et al*.
98 2021). The defects in pluripotency, which underlie the neural tube defects observed in LIN-
99 41/TRIM71 deficient mice, may be highly relevant to the finding of *de novo* heterozygous LIN-
100 41/TRIM71 missense mutations in congenital hydrocephalus cases in humans (Furey *et al*. 2018;
101 Jin *et al*. 2020). Germ cell-specific depletion of LIN-41/TRIM71 in mice causes germ cell loss
102 and sterility in both sexes (Torres-Fernández *et al*. 2021a). Interestingly, male mice with LIN-
103 41/TRIM71-deficient germ cells exhibit a Sertoli cell-only phenotype, which resembles the
104 infertility phenotype of human males with heterozygous LIN-41/TRIM71 mutations (Torres-
105 Fernández *et al*. 2021a). The essential role of LIN-41/TRIM71 in female germ cells remains to
106 be more fully explored. Thus, in mammals, LIN-41/TRIM71 mutations produce distinct
107 phenotypes in germ cells and somatic cells, which highlights the flexibility of LIN-41/TRIM71
108 proteins for deployment in developmental cell fate decisions. Indeed, LIN-41 was first
109 discovered as a target of the *let-7* microRNA in the genetic pathway controlling the
110 developmental timing of somatic cells in *C. elegans* (Reinhart *et al*. 2000; Slack *et al*. 2000). The
111 regulation of LIN-41/TRIM71 orthologs by *let-7* microRNAs appears to be highly conserved in
112 animals (O'Farrell *et al*. 2008; Kloosterman *et al*. 2004; Kanamoto *et al*. 2006; Lin *et al*. 2007;
113 Rybak *et al*. 2009; Worringer *et al*. 2014). This mode of regulation is not observed in the *C.*
114 *elegans* germline, as the *let-7* microRNA appears to be only expressed in somatic cells (Lau *et*
115 *al*. 2001). A new twist is that recent studies suggest that mammalian LIN-41/TRIM71 can inhibit
116 the accumulation of *let-7* microRNAs (Liu *et al*. 2021; Torres-Fernández *et al*. 2021b),
117 suggesting its involvement as a component of a bistable developmental switch. Although it is not

118 known whether LIN-41 can inhibit the *let-7* pathway in *C. elegans*, it is clear that LIN-41 is a
119 component of a bistable switch regulating oocyte meiotic maturation in this organism—LIN-41
120 inhibits CDK-1 activation, and in turn, active CDK-1 promotes the ubiquitin-mediated
121 degradation of LIN-41 upon the onset of meiotic maturation (Spike *et al*. 2018).

122 The rapid elimination of LIN-41 upon the onset of meiotic maturation is emblematic of
123 the highly choreographed and exquisitely timed patterns of degradation of RNA-binding proteins
124 during late oogenesis and the OET in many organisms (Nishi *et al*. 2005; Stitzel *et al*. 2006;
125 Shirayama *et al*. 2006; Sha *et al.* 2017; Kisielnicka *et al.* 2018; Cao *et al*. 2020, 2021; Zavortink
126 *et al*. 2020; reviewed by Robertson and Lin 2015). Previous results suggested that an SCF-type
127 E3 ubiquitin ligase containing the FBW7/Cdc4 ortholog SEL-10 promotes the degradation of
128 LIN-41 using a bi-partite degron located near the N-terminus of LIN-41 (Spike *et al.* 2018). The
129 ubiquitin proteasome pathway utilizes an E1-E2-E3 enzymatic relay to transfer ubiquitin to mark
130 proteins for degradation by the 26S proteasome. E3 ubiquitin ligases, comprising multi-subunit
131 enzymes or single chain proteins, function as substrate specificity factors to conjugate multiple
132 ubiquitin moieties to target proteins. SEL-10 is a highly conserved and well-studied substrate-
133 recognition subunit (Hubbard *et al*. 1997, de la Cova and Greenwald 2012). After substrate
134 proteins are recognized and ubiquitinated, they are received by the 19S regulatory particles of the
135 proteasome, which bind the ubiquitin chains, unfold the substrate, and processively translocate it
136 into the 20S particle for degradation (reviewed by Finley 2009; Collins and Goldberg 2017).

137 In this work, we strengthen our understanding of LIN-41 degradation and begin to
138 investigate how additional RNA-binding proteins in LIN-41 RNPs are degraded upon the onset
139 of meiotic maturation. First, we show that SEL-10 is expressed in oocytes and use
140 photoconversion of DENDRA::LIN-41 in maturing oocytes to demonstrate unequivocally that

141 SEL-10 is required to degrade LIN-41 during the OET. Next, we identify the Pumilio/FBF-
142 family RNA-binding proteins PUF-3 and PUF-11 as proteins that are degraded soon after
143 meiotic maturation. PUF-3 and PUF-11 are components of LIN-41-containing RNPs in oocytes
144 (Tsukamoto *et al*. 2017) that are 89 percent identical at the amino acid level and play important
145 roles in germline stem cell and embryonic development (Hubstenberger *et al.* 2012, Haupt *et al.*
146 2020). Although both PUF-3 and PUF-11 are degraded soon after meiotic maturation in a CDK-
147 1-dependent fashion, the degradation of both proteins occurs independently of SEL-10.
148 Collectively, these results indicate that PUF-3 and PUF-11 are not degraded as a consequence of
149 LIN-41 degradation and that LIN-41 RNPs are dismantled in a concerted fashion during the
150 OET. Finally, we find that several different GFP-tagged fusion proteins that are degraded during
151 the OET, including fusions with PUF-3, PUF-11 and LIN-41, are incompletely degraded when
152 the function of the conserved ETC-1/UBE3C/Hul5 HECT-domain ubiquitin ligase is reduced,
153 indicating that ETC-1 is important for proteasome processivity. We provide evidence that the
154 GFP tag causes this proteolysis defect, re-evaluate key aspects of a previous report that assigned
155 a different role to ETC-1 (Wang *et al*. 2013), and propose that proteasomal processivity is
156 critical for the rapid and efficient targeting of a plethora of oocyte regulatory proteins for
157 degradation during the OET.

158

159 **MATERIALS AND METHODS**

160 ***Strains and genetic analysis***

161 The genotypes of strains used in this study are reported in Table S1. All analyses were conducted
162 at 20 °C, unless specified otherwise. *mat-1(ax161*ts*)* animals are susceptible to even brief
163 observations and manipulations at room temperature. Thus, strains containing the *mat-1(ax161*ts*)*
164 mutation were handled as little as possible (< 15 min at room temperature) and prechilled (15°C)
165 media was used to establish cultures. The following mutations were used: LGI—*rnp-*
166 *8(tn1860[rnp-8::gfp::tev::3xflag])*, *mat-1(ax161*ts*)*, *lin-41(tn1541[gfp::tev::s::lin-41]))*, *lin-*
167 *41(tn1892[mscarlet::tev::3xflag:lin-41])*, *lin-41(tn1894[dendra::tev::3xflag::lin-41])*, *lin-*
168 *41(tn2054[gfp::tev::3xflag::lin-41])*, *lin-41(tn2055[gfp::tev::3xflag::lin-41])*, and *fog-3(q443)*.
169 *lin-41(tn2054)* and *lin-41(tn2055)* were generated independently but are identical at the DNA
170 sequence level. LGII—*dpy-10(tn2076)*, *etc-1(gk5182)*, *etc-1(tn1919[gfp::tev::3xflag::etc-1]),*
171 *etc-1(tn1920[gfp::tev::3xflag::etc-1]), etc-1(tn2077),* and *unc-4(e120)*. LGIII—*plk-1(or683*ts*),*
172 *emb-30(tn377*ts*),* and *cul-2(or209*ts*)*. LGIV—*puf-11(tn1824[puf-11::gfp::tev::3xflag]), puf-*
173 *11(q971)*, *cyb-1(tn1806[cyb-1::gfp::tev::3xflag]), unc-22(e66), puf-3(tn1820[puf-*
174 *3::gfp::tev::3xflag]),* and *puf-3(q966)*. LGV—*lon-3(e2175)*, *sel-10(ar41)*, *sel-10(ok1632)*, *sel-*
175 *10(tn1816[sel-10::gfp::tev::3xflag])*, *sel-10(tn1817[sel-10::gfp::tev::3xflag])*, *sel-*
176 *10(tn1875[gfp::tev::3xflag::sel-10])* and *fog-2(oz40)*. *sel-10(tn1816)* and *sel-10(tn1817)* were
177 generated independently but are identical at the DNA sequence level. The following balancers
178 were used: *tmC18[dpy-5(tmIs1236)]* I (Dejima *et al.* 2018), *mnC1[dpy-10(e128) unc-52(e444)*
179 *umnIs32]* II, *nT1[qIs51]* (IV; V). The following transgene insertions were used: *itIs37[pie-*
180 *1p::mcherry::histoneH2B::pie-1 3'UTR, unc-119(+)]* IV (McNally *et al*. 2006) and *ddIs128[ify-*
181 *1::2xty1::egfp::3xflag(92C12) + unc-119(+)]* (Sarov *et al*. 2012).

182 ***mScarlet and Dendra repair templates***

183 The repair templates used to create *lin-41(tn1892[mscarlet::tev::3xflag::lin-41])* and *lin-*
184 *41(tn1894[dendra::tev::3xflag::lin-41])* were generated by Gibson assembly using the
185 NEBuilder HiFi DNA Assembly master mix (New England Biolabs, Ipswich, MA) and five
186 different PCR products: (1) a *lin-41* 5' homology arm (~0.6 kb), (2) a codon-optimized mScarlet-
187 I or a Dendra coding sequence with introns (~0.9 kb), (3) self-excising cassette (SEC)-containing
188 sequences (~5.7 kb), (4) a *lin-41* 3' homology arm (~0.8 kb), and (5) vector backbone sequences
189 (~2.6 kb). *lin-41* homology arms (1 and 4) were amplified from genomic DNA prepared from the
190 wild type. SEC and vector sequences (3 and 5) were amplified from *Cla*I and *Spe*I-digested
191 pDD268 plasmid DNA (Dickinson *et al*. 2015). mScarlet-I and Dendra were amplified from the
192 plasmids pMS050 (Addgene plasmid #91826), a gift from Bob Goldstein, and pEG545 (Griffin
193 *et al.* 2011), a gift from Geraldine Seydoux. Primer sequences are presented in File S1. All PCR
194 products were initially column purified (Qiagen, Valencia, CA) and most of the plasmids
195 recovered after assembly lacked the SEC fragment; only 10% and 5% of the mScarlet-I and
196 Dendra repair constructs were complete, respectively. While making different *lin-41* repair
197 constructs using the same method and many of the same PCR fragments, we found that gel
198 purifying the SEC PCR product increased the inclusion of the SEC fragment to 80% of the
199 assembled plasmids.

200 Constructs created by Griffin *et al.* (2011) that contain DENDRA-expressing sequences
201 optimized for use in *C. elegans* (Gallo *et al.* 2010) are annotated in Addgene as containing
202 DENDRA2 (e.g., pEG545, Addgene plasmid #40116 and pEG345, Addgene plasmid #40077).
203 DENDRA2 is a modified form of DENDRA that has an important single amino acid change near
204 the C-terminus (A224V) as well as a 5-amino acid insertion near the N-terminus (Gurskaya *et al.*

205 2006; Chudakov *et al.* 2007). The relationship between DENDRA and DENDRA2 is most easily
206 visualized using the fluorescent protein database www.fpbase.org (Lambert 2019). We
207 sequenced the pEG545 plasmid and confirmed that it encodes DENDRA; the DENDRA-coding
208 sequence lacks both the A224V amino acid change and the 5-amino acid insertion found in
209 DENDRA2. Since we obtained pEG545 directly from the Seydoux lab, we also analyzed the
210 Addgene-deposited sequences of pEG545 and pEG345. Although those sequences are
211 incomplete, they confirm that each plasmid encodes DENDRA[A224]. As both plasmids have
212 been used to generate many different fusion proteins labeled as containing DENDRA2 [e.g.,
213 Herrera *et al.* (2016) and Rosu and Orna Cohen-Fix (2017)], this annotation error may be
214 relatively common in the *C. elegans* literature.

215 ***Genome editing***

216 Plasmids that express guide RNAs (gRNAs) under the control of the U6 promoter were
217 generated as described (Arribere *et al*. 2014). Repair templates used to tag genes with *gfp* were
218 also generated as described (Dickinson *et al.* 2015). Repair templates used to tag genes with
219 mSCARLET-I and DENDRA were generated as described in the previous section. Genome
220 editing was performed by injecting wild-type adult gonads with a DNA mix containing a repair
221 template (10 ng/µl), one or more gRNA plasmids (25 ng/µl each), Cas9-expressing plasmid
222 (pDD162, 50 ng/µl), and injection marker (pMyo2::Tdtomato, 4 ng/µl) and selecting for repairs
223 and selection cassette excisions using standard methods (Dickinson *et al*. 2015). Null mutations
224 in *lin-41* are both Dumpy (Dpy) and sterile (Slack *et al.* 2000; Spike *et al.* 2014a). None of the
225 animals homozygous for the *mScarlet^SEC^lin-41*, *Dendra^SEC^lin-41* and *GFP^SEC^lin-41*
226 repairs were Dpy, but some were sterile, consistent with the interpretation that the insertion of
227 each SEC (self-excising cassette) at the 5' end of the *lin-41* gene created reduction-of-function

228 rather than null alleles of *lin-41*. Each *lin-41* repair was balanced with *tmC18* and the SEC was
229 removed from the *lin-41* locus in balanced heterozygotes. Fluorescently tagged *lin-41* alleles
230 were homozygous fertile after SEC excision. All edited loci were validated by sequencing the
231 repair junctions using PCR products as templates. At least two alleles derived from
232 independently injected parents were isolated and assigned allele names. A 4240 bp deletion in
233 the *etc-1* locus, which removes the entire open reading frame was constructed using the *dpy-1*0
234 co-conversion method (Arribere *et al*. 2014). The injection mix contained pJA58 (7.5 ng/µl), AF-
235 ZF-827 (500 nM), etc-1 sgRNA2 (pCS629) (25 ng/µl), etc-1 sgRNA4 (pCS633) (25 ng/µl), the
236 repair template etc-1_RT1 (500 nM), and pDD162 (50 ng/µl). Correct targeting was verified by
237 conducting PCR with primer pairs eif-2Bepsilon_F2 and hgap-2_F2 followed by Sanger
238 sequencing. The DG5379 *dpy-10(tn2076) etc-1(tn2077)* strain was isolated after screening the
239 progeny of 267 F1 Roller animals. The *etc-1(tn2077)* null mutation was separated from the *dpy-*
240 *10(tn2076)* mutation by recombination by seeking non-Dpy non-Rol non-Unc animals from *dpy-*
241 *10(tn2076) etc-1(tn2077)/unc-4(e120)* heterozygotes.

242 ***Antibody staining***

243 Dissected gonads stained with the rabbit anti-GLD-1 primary antibody (1:200 or 1:300 dilution;
244 Jan *et al*. 1999) were fixed in 1% paraformaldehyde for 10 min, with a 5-min post fix step in ice-
245 cold methanol as previously described (Rose *et al.* 1997; Spike *et al.* 2018). Primary antibodies
246 were detected using Cy3-conjugated donkey anti-rabbit secondary antibodies (1:500 dilution;
247 Jackson ImmunoResearch, West Grove, PA).

248

249

250 ***Microscopy and image analysis***

251 Microscope images in Figures 4 and S2 were acquired on a Carl Zeiss motorized Axioplan 2
252 microscope with a 63x Plan-Apochromat (numerical aperture 1.4) objective lens using an
253 AxioCam MRm camera and AxioVision software (Carl Zeiss, Thornwood, NY). Microscope
254 images in Figures S4, 5I–L, S6, S8 and S9 were acquired on a Nikon Ni-E microscope with
255 either a Plan Apo λ 60x (numerical aperture 1.4) objective or a Plan Fluor 40x Oil (numerical
256 aperture 1.3) objective using NIS elements (Nikon Inc., Melville, NY). All the remaining
257 microscope images were acquired on a Nikon Ti2 inverted confocal microscope with a Plan
258 ApoIR 60x objective (numerical aperture 1.27), motorized stage and Galvano scanner using NIS
259 elements (Nikon Inc., Melville, NY). When using the Nikon Ti2 microscope, the large image
260 function of NIS elements was used to acquire images that show the entire germline. We
261 quantified the average fluorescence intensity in selected areas of images using the measure
262 function of ImageJ (Schneider *et al*. 2012). Each measurement was background corrected using
263 the average fluorescence intensity of a nearby area outside the body of the worm. Multiple
264 images were analyzed per genotype, as specified in the text.

265 ***Photoconverting ^{Green}DENDRA::LIN-41 to ^{Red}DENDRA::LIN-41***

266 Worms were mounted without anesthetic on 10% agarose pads in a 1:1 solution of M9 buffer and
267 0.1 μM polystyrene beads (Polysciences, Inc., Warrington, PA) essentially as described (Rosu
268 and Cohen-Fix 2020). Photoactivation and imaging was performed using the Nikon Ti2 inverted
269 confocal microscope equipped as described in the previous section. A region of interest
270 encompassing the −1 oocyte was selected for photoactivation using the 405 nm laser at 10%
271 power for 31.25 seconds (125 loops at 4 frames per second) and a large pinhole (173.69 microns)

272 to promote DENDRA photoconversion throughout the oocyte. After photoactivation, animals
273 were allowed to recover on NGM plates seeded with OP50-1 bacteria for either 60 min or 100
274 min and then mounted a second time. Confocal settings optimized to image oocytes after
275 photoconversion were used to collect images of the ^{Green}DENDRA::LIN-41 and
276 ^{Red}DENDRA::LIN-41 in oocytes and embryos at all stages of the experiment: before
277 photoactivation, after photoactivation, and after recovery.

278 Although the conditions used for photoactivation were generally compatible with oocyte
279 meiotic maturation and ovulation, our experimental manipulations sometimes interfered with
280 these events. For example, one *lin-41(tn1894)* animal failed to move after recovery, suggesting
281 that it might have been damaged while mounting on or recovering from the agarose pad.
282 ^{Red}DENDRA::LIN-41 was still detectable in the −1 and −2 oocytes of the photoconverted arm
283 after a 100-min recovery period, indicating that the converted oocytes in this damaged animal
284 had not matured or ovulated. The other *lin-41(tn1894)* animals (n=5) survived the experimental
285 manipulations and exhibited exclusively green oocytes in the −1 and −2 positions in each
286 photoconverted arm (n=6 arms, the −1 oocytes of both arms were converted in one animal),
287 confirming that oocytes had matured and been ovulated into the uterus during the recovery
288 period (60 min (n=2) or 100 min (n=4)). All *lin-41(tn1894); sel-10(ok1632)* animals survived
289 our experimental manipulations (n=4 animals), and most of the photoconverted arms had
290 exclusively green oocytes in the −1 and −2 positions (n=4/5 arms, the −1 oocytes of both arms
291 were converted in one animal) and one or two red embryos in the uterus after the recovery
292 period. The sole exception was in an animal that laid only 2 eggs during the 100-min recovery
293 period and appeared to be sickly. This animal had a bright red 1-cell stage embryo in the +1
294 position and a fainter red oocyte in the −1 position. The −1 oocyte converted in this gonad arm

295 must have experienced a substantial temporal delay prior to oocyte maturation and ovulation, as
296 a shorter (60 min) recovery period was sufficient for two ovulation events in the healthier *lin-*
297 *41(tn1894); sel-10(ok1632)* animals.

298 ***itIs37 puf-3(tn1820) and puf-11(tn1824) puf-3(tn1820) double mutants***

299 Crosses with *puf-11(tn1824)* and *puf-3(tn1820)* established that the *itIs37[pie-*
300 *1p::mcherry::histoneH2B::pie-1 3'UTR, unc-119(+)]* insertion on chromosome IV is tightly
301 linked to *puf-11* and more loosely linked to *puf-3*. 0 of 72 progeny from *itIs37* + / + *puf-*
302 *11(tn1824)* parents carried a recombinant *itIs37 puf-11(tn1824)* chromosome, while 5 of 64
303 progeny from *itIs37* + / + *puf-3(tn1820)* parents carried a recombinant *itIs37 puf-3(tn1820)*
304 chromosome. Together, these observations suggested that *itIs37* is ~7.8 map units to the left of
305 *puf-3*, in good agreement with the relative genetic positions of *puf-11* and *puf-3* described in
306 WormBase (http://www.wormbase.org, release WS278; Davis *et al*. 2022). We utilized *unc-*
307 *22(e66)*, which causes a homozygous Uncoordinated (Unc) phenotype and is located in-between
308 *puf-11* and *puf-3*, to construct the *puf-11(tn1824) puf-3(tn1820)* double mutant. Animals carrying
309 *itIs37 puf-3(tn1820)* and *puf-11(tn1824) unc-22(e66)* recombinant chromosomes were mated
310 with each other. Animals with one copy of each chromosome were selected and allowed to self-
311 fertilize. In the next generation, non-Unc-22 animals were examined for *itIs37*-derived
312 mCHERRY::HISTONE expression using fluorescence microscopy. A single *itIs37*-negative
313 animal was identified among the 168 non-Unc animals examined, and this animal segregated
314 approximately one quarter Unc progeny in the next generation. Based on the mapping data, we
315 anticipated that this rare animal carried either a *puf-11(tn1824) puf-3(tn1820)* or a *puf-11(+) puf-*
316 *3(tn1820)* recombinant chromosome in *trans* to the parental *puf-11(tn1824) unc-22(e66)*
317 chromosome. Animals homozygous for the recombinant chromosome were analyzed using

318 primers that produce allele-specific PCR products (File S1) and found to carry both *puf-*
319 *11(tn1824)* and *puf-3(tn1820)*.

320 ***RNA interference***

321 Gene-specific RNA interference (RNAi) was performed by feeding *C. elegans* with double-
322 stranded RNA (dsRNA)-expressing *E. coli* (Timmons and Fire 1998) at 22 °C using the RNAi
323 culture media described by Govindan *et al*. (2006). RNAi clones were obtained from Source
324 BioScience (Nottingham, UK), and the identities of important RNAi clones were verified by
325 DNA sequencing (see File S1 for details). Exposure to dsRNA-expressing *E. coli* was initiated
326 during the fourth larval stage and animals were examined and imaged after 2 days. Under these
327 RNAi conditions and at the time-point analyzed, all *cdk-1(RNAi)* animals produced arrested 1-
328 cell embryos and therefore had a strong *cdk-1(RNAi)* phenotype (see Boxem *et al.* 1999). Using
329 the same RNAi conditions, the gonad arms of *wee-1.3(RNAi)* animals exhibited a range of oocyte
330 phenotypes. Gonads with a mild *wee-1.3(RNAi)* phenotype have relatively large and normal-
331 appearing oocytes that occupy approximately normal positions with respect to each other and to
332 the spermatheca. Gonads with strong *wee-1.3(RNAi)* phenotype have small, sometimes indistinct
333 oocytes or a mass of oocyte-like material near the spermatheca. Burrows *et al.* (2006) also noted
334 that prolonged RNAi results in small oocytes, consistent with the idea that this phenotype is
335 caused by a strong response to *wee-1.3(RNAi)*. GFP_S::LIN-41 is prematurely degraded in animals
336 with both weak and strong *wee-1.3(RNAi)* phenotypes (Spike *et al.* 2014a, 2018). In the screen
337 for E3 ubiquitin ligases that degrade PUF-3::GFP, we did not exclusively use RNAi to test the
338 SCF subunit CUL-2. Since our *cul-2(RNAi)* clone does not trigger a good RNAi response (Spike
339 *et al*. 2018), we also examined *cul-2(or209*ts*)*; *puf-3(tn1820[puf-3::gfp::tev::3xflag])* adults 1

340 day after they were upshifted to 25 °C as L4-stage larvae. All other ubiquitin ligase subunits
341 were screened using RNA interference alone.

342 ***Western blots***

343 Each lane was loaded with a protein lysate made from adult worms picked into 10 microliters of
344 phosphate-buffered saline (PBS) containing proteinase inhibitors (2x complete EDTA-free;
345 Millipore-Sigma, St. Louis, MO). Whole-worm lysates were frozen at –80 °C and prepared for
346 electrophoresis by adding LDS sample buffer supplemented with a reducing agent (Invitrogen,
347 Carlsbad, CA). Immediately after adding the sample buffer, the samples were heated at 70 °C
348 and vortexed multiple times prior to loading on a gel. Lysates were made from 40 Day 1 adult
349 worms (24 hours past the L4 stage at 20 °C) with a few exceptions. Some lysates expressing
350 CYB-1::GFP were made from 50 instead of 40 worms (hermaphrodites in Figures 7A and S7B;
351 males in Figures 7B and S7D). In addition, the mated females used for lysates were not
352 developmentally staged (Figure S7C). Instead, gravid females were selected from mixed-stage
353 plates. Proteins were separated using 3–8% Tris-Acetate gels (Invitrogen, Carlsbad, CA) and
354 visualized after western blotting. Blots were blocked with 5% nonfat dried milk. The primary
355 antibodies used were mouse anti-FLAG M2 (Millipore-Sigma) at a 1:2,000–1:4,000 dilution and
356 rabbit anti-GFP NB600-308 (Novus Biologicals, Littleton, CO) at a 1:4,000 dilution. The
357 secondary antibodies used were peroxidase-conjugated goat anti-mouse (Thermo Scientific,
358 Waltham, MA) at a 1:30,000 dilution or peroxidase-conjugated donkey anti-rabbit (Thermo
359 Scientific) at a 1:5,000 dilution. Detection was performed using SuperSignal West Femto
360 Maximum Sensitivity Substrate and CL-XPosure film (Thermo Scientific).

361

362 ***eGFP, mSCARLET-I and DENDRA fusion protein tag sequences***

363 The predicted amino sequence and molecular mass of each protein tag is presented in File S2 for
364 reference. All GFP tags express the GFP[S65C] enhanced GFP variant commonly used in *C.*
365 *elegans* (Green *et al.* 2008). Most also contain the apparently neutral GFP[Q80R] change likely
366 introduced into the original GFP cDNA sequence by PCR error (Tsien 1998).

367 ***Data availability***

368 All alleles and strains (Table S1), plasmids (File S1) and Sanger sequencing files are available
369 upon request. Primer sequences are provided in File S1. File S2 contains the amino acid and
370 nucleotide sequences of fluorophore tags, tagged alleles, and deletion alleles created for or used
371 in this work. Supplemental materials are available at Figshare: https://doi.org/

372

373 **RESULTS**

374 ***SEL-10 is present in the cytoplasm and nucleoplasm of oogenic germ cells***

375 SEL-10/Cdc4/FBW7 is a highly conserved F-box protein; it is the substrate-recognition subunit
376 of a Skp, Cullin, F-box (SCF)-containing E3 ubiquitin ligase complex that promotes the
377 ubiquitination and degradation of specific substrates (reviewed in Deshaies and Ferrell 2001;
378 Welcker and Clurman 2008). In *C. elegans*, SEL-10 functions in the oogenic germline and
379 during the OET to promote the timely elimination of the cytoplasmic RNA-binding proteins
380 GLD-1 and LIN-41 at different stages of oogenesis (Kisielnicka *et al*. 2018; Spike *et al.* 2018).
381 Consistent with this idea, *sel-10* mRNA is expressed throughout the oogenic germlines of adult
382 hermaphrodites and the *sel-10* 3' UTR is permissive for the translation of green fluorescent
383 protein (GFP) in pre-meiotic and meiotic cells during oogenesis (Kisielnicka *et al.* 2018).
384 However, the expression of SEL-10 has not been reported in oocytes or in any other region of the
385 *C. elegans* germline, possibly because SEL-10 expression constructs were examined in the
386 context of extrachromosomal arrays (Ding *et al.* 2007; Dorfman *et al.* 2009), which can silence
387 the expression of germline genes in *C. elegans* (Kelly *et al.* 1997). To avoid this technical issue,
388 we used genome editing to generate new alleles of *sel-10* that have a GFP-tag fused to the SEL-
389 10 protein at both the amino-terminus (N-terminus, GFP_F::SEL-10 in Figure 1) and carboxyl-
390 terminus (C-terminus, SEL-10::GFP_F in Figure 1). In the figures, and where needed for textual
391 clarity, we will indicate the presence and relative position of a 3xFLAG or an S epitope tag in a
392 fusion protein with an F or S subscript, respectively. The alleles that express GFP::SEL-10, SEL-
393 10::GFP, and many of the other fusion proteins used in this work, are shown in Figure S1.

394 The pattern of GFP expression from each *sel-10* allele confirms that SEL-10 is expressed
395 throughout the oogenic germline of adult hermaphrodites and in early embryos (Figure 1, C and
396 E). GFP::SEL-10 and SEL-10::GFP are present in the nucleoplasm and cytoplasm of oocytes and
397 distal germ cells, but show different patterns of localization, likely reflecting the fact that
398 GFP::SEL-10 is functional, whereas SEL-10::GFP is not, as described in the subsequent section.
399 GFP::SEL-10 is enriched in the nucleoplasm relative to the cytoplasm at all stages of germ cell
400 development (Figure 1C). GFP::SEL-10 localization throughout the distal region of the gonad
401 appears to be "ring-like" because it is enriched in the nucleoplasm relative to the cytoplasm and
402 largely excluded from nucleoli (Figure 1, C and G–I). SEL-10::GFP is also excluded from
403 nucleoli at all stages of germ cell development (Figure 1, E and J–L). However, SEL-10::GFP is
404 present at similar levels in the nucleoplasm and cytoplasm of distal germ cells and only becomes
405 enriched in the nucleoplasm of growing oocytes (Figure 1E). Using confocal images collected
406 with identical settings, we measured 23% and 43% increases in background-corrected
407 cytoplasmic fluorescence in the rachis and the –3 oocyte, respectively, in SEL-10::GFP animals
408 relative to GFP::SEL-10 animals ($P<0.01$, n=7 images per genotype). However, nuclear
409 fluorescence in the –3 oocyte of each strain was not significantly different ($P>0.1$). We conclude
410 that, at least in the oogenic germline, SEL-10::GFP appears to be more abundant than GFP::SEL-
411 10 and more likely to reside in the cytoplasm.

412

413 ***GFP::SEL-10 is functional but SEL-10::GFP is not***

414 The different patterns of GFP::SEL-10 and SEL-10::GFP localization might reflect the
415 disruption or alteration of SEL-10 function by the inserted protein tags. We examined the

416 accumulation of LIN-41 and GLD-1 in animals homozygous for each GFP-tagged allele of *sel-*
417 *10* to address this possibility. LIN-41 was monitored using *lin-41(tn1892[mscarlet::3xflag::lin-*
418 *41])*, a new allele of *lin-41* that produces a fusion protein with an mSCARLET-tag fused to the
419 N-terminus of LIN-41 (Figure S1B; mSC_F::LIN-41). Endogenous GLD-1 levels were analyzed
420 by immunostaining. mSCARLET::LIN-41 is strongly expressed in wild-type and *sel-10(ok1632)*
421 loss-of-function mutant oocytes (Figure 1, A and B). mSCARLET::LIN-41 is down-regulated in
422 wild-type embryos (Figure 1A), but persists at elevated levels in the embryos produced by *sel-*
423 *10(ok1632)* mutant animals (Figure 1B). The downregulation of mSCARLET::LIN-41 protein
424 expression during the OET is therefore SEL-10-dependent, as described for endogenous LIN-41
425 and a GFP-tagged LIN-41 fusion protein (Figure S1B; GFP_S::LIN-41; Spike *et al*. 2018).
426 mSCARLET::LIN-41 is downregulated in the embryos of GFP::SEL-10-expressing animals (*sel-*
427 *10(tn1875)*, Figure 1D), but persists at elevated levels in the embryos of SEL-10::GFP-
428 expressing animals (*sel-10(tn1817)*, Figure 1F). Similar results were observed with GLD-1
429 (Figure S2). GLD-1 is downregulated as developing oocytes exit pachytene near the loop region
430 (Figure S2, A and C), and this process is impaired in *sel-10(lf)* mutants, resulting in elevated
431 levels of GLD-1 in proximal oocytes (Kisielnicka *et al.* 2018; Spike *et al.* 2018). GLD-1 is
432 downregulated in the oocytes of GFP::SEL-10-expressing animals (*sel-10(tn1875)*, Figure S2B),
433 but persists at elevated levels in the oocytes of SEL-10::GFP-expressing animals (*sel-10(tn1816)*,
434 Figure S2D). We conclude that at least two of the normal functions of SEL-10 are compatible
435 with the insertion of a GFP tag at the N-terminus of SEL-10 but are disrupted by the insertion of
436 a GFP tag at the SEL-10 C-terminus. Furthermore, these observations suggest that the
437 nucleoplasm-enriched localization pattern of GFP::SEL-10 shown in Figure 1C likely represents
438 the correct localization pattern of SEL-10 in the oogenic germline. Although known targets of

439 SEL-10 in the *C. elegans* germline are predominantly cytoplasmic (e.g., LIN-41, GLD-1 and
440 CPB-3 (Kisielnicka *et al.* 2018; Spike *et al.* 2018)), orthologs of SEL-10 are present in the
441 nucleoplasm in *S. cerevisiae* (Cdc4p) (Choi *et al.* 1990) and in both the nucleoplasm and
442 cytoplasm in humans (FBW7α and FBW7β isoforms, respectively) (Welcker *et al.* 2004).

443

444 ***SEL-10 is required to degrade LIN-41 during the OET***

445 LIN-41 disappears rapidly upon the onset of meiotic maturation. We previously hypothesized
446 that LIN-41 is phosphorylated at this stage and recognized by a SEL-10-containing E3 ubiquitin
447 ligase that targets LIN-41 for proteolysis (Spike *et al*. 2018). To confirm that SEL-10 promotes
448 the degradation of LIN-41 during the OET, we generated *lin-41(tn1894[dendra::3xflag::lin-*
449 *41])*, a new allele of *lin-41* that produces a protein with a DENDRA-tag fused to the LIN-41 N-
450 terminus (Figure S1B; DND_F::LIN-41) and crossed it into a *sel-10(ok1632)* mutant background.
451 Photoactivation irreversibly converts the fluorescence emitted by DENDRA from green to red
452 (^{Green}DENDRA and ^{Red}DENDRA, respectively) (Gurskaya *et al*. 2006). The ^{Green}DENDRA::LIN-
453 41 present in the −1 oocytes of *sel-10(ok1632)* and *sel-10(+)* animals was targeted for
454 conversion to ^{Red}DENDRA::LIN-41 using a 405 nm laser. Robust photoconversion was observed
455 in the −1 oocyte, with a small amount of red fluorescence sometimes visible in the adjacent
456 cytoplasm of the −2 oocyte (Figure 2, A, B, F, and G). After a suitable recovery period to permit
457 oocyte maturation, ovulation, and some embryonic development, bright ^{Red}DENDRA::LIN-41
458 was evident in a single embryo in the uterus of *sel-10(ok1632)* animals (Figure 2, C–E; n=5/5).
459 In general, we noted that the next-youngest embryo (or −1 oocyte in one animal, see Materials
460 and Methods) also contained ^{Red}DENDRA::LIN-41 (n=4/5), but at a much lower level. We did

461 not observe bright ^{Red}DENDRA::LIN-41 in any of the embryos in the uteri of *sel-10(+)* animals
462 (n=6), although we sometimes saw an embryo with a slight haze of red fluorescence that we
463 hypothesized might be derived from the converted ^{Red}DENDRA::LIN-41 −1 oocyte (Figure 2, H
464 and I). Relative to these *sel-10(+)* embryos, we measured a 6- to 10-fold higher level of
465 background-corrected ^{Red}DENDRA::LIN-41 fluorescence in the brightest *sel-10(ok1632)*
466 embryos (n=4 of each genotype). Together, these results indicate that the fluorescently tagged
467 ^{Red}DENDRA::LIN-41 observed in *sel-10(ok1632)* embryos originates in oocytes and confirm
468 that LIN-41 is degraded during the OET in wild-type animals.

469

470 ***PUF-3 and PUF-11 are degraded during the OET***

471 PUF-3 and PUF-11 are nearly identical Pumilio-family RNA-binding proteins that function
472 redundantly with respect to normal embryonic development in *C. elegans* (Hubstenberger *et al.*
473 2012; Haupt *et al.* 2020). PUF-3 and PUF-11 proteins and mRNAs co-purify with LIN-41-
474 containing ribonucleoprotein (RNP) complexes (Tsukamoto *et al.* 2017). Furthermore, LIN-41
475 and PUF-3/11 were each identified as factors important for the 3'UTR-mediated translational
476 repression of the Rbfox-related RNA-binding protein SPN-4 in oocytes (Hubstenberger *et al.*
477 2012; Tsukamoto *et al*. 2017). These observations suggest that LIN-41, PUF-3, and PUF-11
478 function together in developing oocytes. We confirmed that PUF-3 and PUF-11 are expressed in
479 oocytes, as described (Haupt *et al.* 2020), and also examined the expression patterns of PUF-3
480 and PUF-11 during the oocyte-to-embryo transition. We created new alleles of *puf-3* and *puf-11*
481 that fuse a GFP-tag to the C-terminus of each PUF protein (Figure S1C; PUF-3::GFP$_F$ and PUF-
482 11::GFP$_F$) and found that PUF-3 and PUF-11 are eliminated during the OET in a manner that

483 resembles LIN-41 (Figure 3). PUF-3::GFP and PUF-11::GFP are abundant in oocytes, but the
484 expression of each protein is strongly diminished soon after oocyte meiotic maturation and
485 ovulation (Figure 3, A and D; Figure S3, A and B). Consequently, PUF-3::GFP and PUF-
486 11::GFP appear to be largely absent from embryos (Figure 3A) or limited to a single young
487 embryo (Figure 3D and Figure S3, A and B). A similar pattern is observed with GFP::LIN-41
488 and mSCARLET::LIN-41 (Spike *et al.* 2018; Figure 1A). Moreover, PUF-3::GFP or PUF-
489 11::GFP and mSCARLET::LIN-41 identify the same young embryos (if present, as in Figure 3,
490 D and E; n≥7 animals of each genotype imaged as shown). To determine when PUF-3 is
491 eliminated from embryos, we examined PUF-3::GFP in oocytes and embryos that express an
492 mCHERRY::HISTONE fusion protein. Relative to the adjacent −1 oocyte, PUF-3::GFP levels
493 are substantially reduced in meiotic embryos that are in metaphase I (Figure 3, G–J) and most
494 PUF-3::GFP appears to be eliminated by the end of the first meiotic division (Figure 3K). This
495 roughly corresponds to the time window during which LIN-41 is degraded; time-lapse imaging
496 previously demonstrated that GFP::LIN-41 is dramatically reduced by the end of the first meiotic
497 division (Spike *et al.* 2018).

498 While LIN-41, PUF-3 and PUF-11 are strongly reduced soon after meiotic maturation
499 and ovulation, each protein has a distinct pattern of expression in the adult germline (Figure 3,
500 A–F). For example, the accumulation of PUF-3::GFP and PUF-11::GFP appears to peak at a
501 later stage of oogenesis than mSCARLET::LIN-41 (Figure 3, C and F). In addition, PUF-
502 11::GFP is distinctly more abundant than PUF-3::GFP in the distal germline (compare Figure 3,
503 A and D; Figure S3D). Haupt *et al.* (2020) also observed higher levels of PUF-11 in the distal
504 germline using alleles that express V5 epitope-tagged PUF-3 and PUF-11 proteins. Because *puf-*
505 *3* and *puf-11* are redundant, to assess the function of the fusion proteins, we screened for and

506 identified a recombinant that expresses both PUF-3::GFP and PUF-11::GFP using standard
507 genetic methods (see Materials and Methods). As expected from the individual expression
508 patterns, GFP expression was approximately two-fold higher in the oocytes of these animals
509 [*puf-11(tn1824) puf-3(tn1820)* genotype] than in the oocytes of either parent [*puf-11(tn1824)* or
510 *puf-3(tn1820)* alone], and the level of GFP expression in the distal germline was similar to the
511 PUF-11::GFP-expressing strain (Figure S3, A–E). *puf-11(tn1824) puf-3(tn1820)* animals are
512 overtly wild-type; they are homozygous viable and fertile, with a brood size similar to the wild
513 type (333 ± 40 larvae, n=15 animals at 20 °C). In addition, most of the embryos produced by *puf-*
514 *11(tn1824) puf-3(tn1820)* animals hatch (~1% embryonic lethality). Since animals that are
515 doubly homozygous for deletion alleles of *puf-11* and *puf-3* [*puf-11(q971) puf-3(q966)* animals]
516 exhibit maternal-effect embryonic lethality (Haupt *et al.* 2020), the GFP-tagged alleles of *puf-11*
517 and *puf-3* must retain some wild-type function. As a more stringent test, we crossed homozygous
518 *puf-11(tn1824) puf-3(tn1820)* males to balanced *puf-11(q971) puf-3(q966) / nT1[qIs51]*
519 hermaphrodites to generate *puf-11(tn1824) puf-3(tn1820) / puf-11(q971) puf-3(q966)* animals.
520 Animals with this genotype produced many embryos that were viable (n=25 animals). We
521 conclude that the GFP tag inserted at the C-terminus of PUF-3 and PUF-11 is largely compatible
522 with the function of each protein.

523

524 ***PUF-3 and PUF-11 are degraded in response to active CDK-1***

525 LIN-41 is degraded in response to meiotic resumption and the activation of the cyclin-dependent
526 kinase CDK-1 (Spike *et al.* 2014a, 2018). Likewise, we find that using RNA interference (RNAi)
527 to strongly reduce CDK-1 activity causes PUF-3::GFP and PUF-11::GFP to persist in embryos

528 (Figure 4, A and E; n>65 for each PUF::GFP with 100% penetrance). Furthermore, a strong
529 RNAi-mediated reduction in the activity of the WEE-1.3 kinase, a negative regulator of CDK-1
530 (Burrows *et al*. 2006), causes oocytes to downregulate PUF-3::GFP and PUF-11::GFP
531 prematurely (Figure 4, B and F). The latter phenotype was partially penetrant; it was observed in
532 32/46 of the PUF-3::GFP and 25/44 of the PUF-11::GFP-expressing *wee-1.3(RNAi)* gonads and
533 mainly seen in *wee-1.3(RNAi)* animals with highly abnormal oocytes. GFP::LIN-41 is also
534 degraded prematurely after *wee-1.3(RNAi)*, but this can be seen in gonads with relatively normal
535 oocytes (Spike *et al.* 2014a), suggesting that LIN-41 might be more sensitive to CDK-1 activity.
536 We tested this idea by treating animals that co-express mSCARLET::LIN-41 and PUF-11::GFP
537 with *wee-1.3(RNAi)* and selectively examining gonads with large, well-organized oocytes. In
538 these animals, mSCARLET::LIN-41 was down-regulated in younger (more distal) oocytes
539 (Figure 4I) and, as a consequence, prematurely eliminated from oocytes more frequently than
540 PUF-11::GFP (in 11/12 instead of 6/12 gonads, respectively). Collectively, these results indicate
541 that active CDK-1 promotes the elimination of PUF-3 and PUF-11 and suggest that LIN-41
542 might be more sensitive to the dysregulatory effects of *wee-1.3(RNAi)*.

543

544 ***SCF_{SEL-10} and APC ubiquitin ligases do not target PUF-3 or PUF-11 for degradation***

545 PUF-3 and PUF-11 are components of LIN-41 RNPs and appear to be eliminated in response to
546 the same signal and at a similar time as LIN-41. We therefore asked whether they are targeted for
547 elimination by the same SCF E3 ubiquitin ligase. LIN-41 persists in early embryos after the
548 RNAi-mediated knockdown of the highly similar Skp-related genes *skr-1* and *skr-2,* the Cullin
549 *cul-1*, the F-box substrate recognition subunit *sel-10* and in the *sel-10(lf)* mutants *sel-10(ok1632)*

550 and *sel-10(ar41)* (Spike *et al*. 2018). However PUF-3::GFP and PUF-11::GFP are eliminated
551 normally from the embryos of *lon-3(e2175) sel-10(ar41)* mutant animals (Figure 4, C, D, G, and
552 H) and after *skr-1/2(RNAi)* (Figure S4, C and I, n>40 animals for each PUF::GFP fusion protein)
553 and *cul-1(RNAi)* (Figure S4, B and H, n≥20 animals for each PUF::GFP fusion protein). A
554 distinct, SEL-10-independent mechanism must therefore promote the elimination of PUF-3 and
555 PUF-11 from early embryos. Furthermore, this indicates that the degradation of PUF-3 and PUF-
556 11 during the OET is not a consequence of the SEL-10-dependent degradation of LIN-41,
557 consistent with our data suggesting that LIN-41 is more sensitive to *wee-1.3(RNAi)* and the idea
558 that multiple mechanisms remodel and take apart oocyte RNPs during the OET.

559 An interesting feature of LIN-41 degradation is that it occurs even when the metaphase-
560 to-anaphase transition of the first meiotic division is blocked by disrupting the function of the
561 anaphase-promoting complex (APC) (Spike *et al.* 2014a). This feature distinguishes LIN-41
562 from proteins such as IFY-1/Securin (Kitagawa *et al.* 2002; Wang *et al.* 2013) and CYB-
563 1/Cyclin B1 (Liu *et al.* 2004), which are degraded slightly later than LIN-41 in an APC-
564 dependent fashion. Therefore, we tested whether the metaphase-to-anaphase transition regulates
565 the elimination of PUF-3::GFP by impairing the function of two key members of the APC, *mat-*
566 *1*/Apc3 and *emb-30*/Apc4 (Furuta *et al.* 2000; Shakes *et al.* 2003). *mat-1(RNAi)* caused fully
567 penetrant 1-cell embryonic arrest, but did not delay or prevent the elimination of PUF-3::GFP
568 from embryos (Figure S4D; n=34 animals). Likewise, PUF-3::GFP disappears normally from the
569 embryos of *emb-30(tn377*ts*)* mutants shifted to 25 °C at the L4 stage (Figure S4F; n > 35); these
570 embryos arrest in metaphase during the first meiotic division (Furuta *et al.* 2000). PUF-11::GFP
571 degradation was also unaffected by *mat-1(RNAi)* (Figure S4J; n=9). We conclude that, as for
572 LIN-41, the elimination of either PUF-3 or PUF-11 from early embryos does not require the

573 activity of the APC. However, unlike LIN-41, the elimination of PUF-3::GFP and PUF-11::GFP
574 from embryos is *sel-10* independent.

575

576 ***ETC-1/Hul5/UBE3C promotes efficient protein clearance during the OET***

577 Since PUF-3/11 are degraded in a SEL-10-independent manner, and because regulated protein
578 degradation often requires ubiquitination (reviewed by Dikic *et al.* 2017), we tested whether a
579 different E3 ubiquitin ligase might promote the elimination of PUF-3::GFP from embryos. Many
580 potential ubiquitin ligases have been identified in *C. elegans*, including (1) multi-subunit E3s
581 (SCF-type, APC), (2) HECT-domain E3s, (3) U-box E3s, and (4) more than 100 RING-finger
582 proteins that might function as monomeric E3s (Kipreos *et al.* 2005). We performed a small-
583 scale RNAi screen that targeted the first three classes of ubiquitin ligases and identified the
584 HECT-domain ubiquitin ligase ETC-1/Hul5/UBE3C as a promising candidate. When animals
585 expressing both mSCARLET::LIN-41 and PUF-3::GFP [*lin-41(tn1892); puf-3(tn1820)*
586 genotype] were exposed to *etc-1(RNAi)*, there was no discernable change in mSCARLET::LIN-
587 41 degradation, yet elevated levels of GFP were observed in multiple young embryos (n=24/24
588 animals). This suggested that *etc-1* knock down specifically interferes with the elimination of
589 oocyte-expressed PUF-3::GFP but not mSCARLET::LIN-41. We confirmed these RNAi-based
590 observations with *etc-1(gk5182)*, a predicted loss-of-function allele, which introduces a
591 premature stop codon, generated by the *C. elegans* Reverse Genetics Core Facility at the
592 University of British Columbia (The *C. elegans* Deletion Mutant Consortium 2012). *etc-*
593 *1(gk5182); puf-3(tn1820)* and *etc-1(gk5182); puf-11(tn1824)* animals exhibit GFP fluorescence
594 in multiple embryos compared to *etc-1(+)* controls (Figure 5, A–D), while expanded

595 mSCARLET is not observed in *lin-41(tn1892); etc-1(gk5182)* animals (Figure 5, E and F).
596 However, detailed analysis presented in subsequent sections suggests that ETC-1 unlikely
597 functions as an E3 ubiquitin ligase that targets specific proteins for degradation during the OET
598 but instead functions as a factor that increases the processivity of the proteasome.

599 ETC-1 was proposed to function as an E3 ubiquitin ligase that regulates the level of
600 cytoplasmic IFY-1/Securin and CYB-1/cyclin B1 in post-meiosis I embryos in *C. elegans* (Wang
601 *et al.* 2013). In that study, RNA interference was used to reduce *etc-1* function [*etc-1(RNAi)*] and
602 CYB-1 degradation was monitored using a transgene that uses heterologous regulatory elements
603 to drive the expression of a GFP::CYB-1 fusion protein in the *C. elegans* germline (*ekIs2[pie-*
604 *1p::gfp::cyb-1]*). We used a new viable and fertile allele of *cyb-1* that expresses a GFP-tagged
605 CYB-1 fusion protein (Figure S1C; CYB-1::GFP_F) to examine CYB-1::GFP expression in wild-
606 type and in *etc-1(gk5182)* embryos (Figure 5, G and H). Since CYB-1 is essential for viability
607 (van der Voet *et al.* 2009), the CYB-1::GFP fusion protein made by *cyb-1(tn1806[cyb-*
608 *1::gfp::3xflag])* homozygotes must be substantially functional *in vivo*. In otherwise wild-type
609 animals, CYB-1::GFP is reduced in young mitotic embryos relative to meiotic embryos and
610 oocytes (Figure 5G). However, in *etc-1(gk5182); cyb-1(tn1806)* embryos GFP levels continue to
611 remain high after meiosis (Figure 5H). We also confirmed that *etc-1(gk5182)* affects the
612 degradation of IFY-1::GFP (IFY-1::GFP_F) using the fosmid-based transgene *ddIs128[ify-*
613 *1::gfp::3xflag]* (Sarov *et al.* 2012). *etc-1(gk5182)* appears to have a relatively weak effect on
614 IFY-1::GFP (Figure 5, I and J) compared to PUF-3::GFP, PUF-11::GFP and CYB-1::GFP
615 (Figure 5, A–D and G–H). The amount of GFP fluorescence in post-meiotic *etc-1(gk5182);*
616 *ddIs128* embryos is only slightly elevated relative to *etc-1(+)* control embryos (Figure 5, I and
617 J). We quantified this modest increase by comparing the IFY-1::GFP fluorescence levels in +2

618 embryos from *etc-1(gk5182)* animals and *etc-1(+)* controls and found it to be increased 1.4-fold
619 in *etc-1* mutants ($P<1x10^{-4}$, *t*-test; n=12 for each genotype).

620

621 ***ETC-1 is broadly expressed and present in oocytes and early embryos***

622 ETC-1 and its orthologs, Hul5 (yeast) and UBE3C (humans) have two well-defined structural
623 domains: an IQ domain close to the N-terminus and a HECT domain at the extreme C-terminus
624 (Figure 6A; Wang *et al.* 2013; Marín 2018). The HECT domain of UBE3C and other HECT-
625 domain E3 ubiquitin ligases has a well-defined function; it is essential for mediating the
626 acceptance and transfer of ubiquitin from an E2-conjugating enzyme to a degradation substrate
627 via a cysteine residue at its catalytic site (You and Pickart 2001; Singh and Sivaraman 2020;
628 reviewed in Lorenz 2018). The IQ domain-containing N-terminus of UBE3C mediates an
629 interaction with the proteasome that is also important for function, but this portion of UBE3C is
630 less well-conserved than the HECT domain and its function is less well-defined (You and Pickart
631 2001; You *et al.* 2003; Wang *et al*. 2013). Given this structural and functional information, we
632 decided to tag the extreme N-terminus with GFP to examine where ETC-1 is expressed and
633 localized in *C. elegans*.

634 When we examined the sequences at the 5' end of the *etc-1* gene (Figure 6A) it became
635 apparent that ETC-1 translation might begin 60 bp upstream of the annotated start codon (ATG
636 #2 in Figure 6A) (http://www.wormbase.org, release WS278). *etc-1* is the downstream gene in a
637 two gene operon and contains an annotated and sequence-verified trans-splice acceptor site
638 immediately adjacent to a possible start codon (ATG #1 in Figure 6A). In *C. elegans*, trans-
639 splicing is used to physically separate the co-transcribed messenger RNAs of an operon (Spieth

640 *et al.* 1993). We predicted that ETC-1 translation should be initiated at ATG #1 for the following
641 reasons: (1) start codons are commonly found within 10 bp of a trans-splice acceptor site (Allen
642 *et al*. 2011), and (2) after trans-splicing, ATG #1 would be the first start codon in the *etc-1*
643 mRNA. If correct, 20 additional amino acids would be appended to the N-terminus of the
644 predicted ETC-1 protein. Seven of these amino acids are similar or identical to equivalent
645 residues at the N-terminus of UBE3C (Figure 6B). We created two different GFP-tagged alleles
646 of *etc-1*: (1) *etc-1(tn1919[gfp::3xflag::etc-1#1])*, which places GFP (and another start codon)
647 immediately upstream of the start codon adjacent to the trans-splice acceptor site (ATG #1), and
648 (2) *etc-1(tn1920[gfp::3xflag::etc-1#2])*, which places an identical tag immediately upstream of
649 the annotated start codon (ATG #2) (Figure S5A). Both *etc-1(tn1919)* and *etc-1(tn1920)* express
650 GFP (Figure 6, C and D, and Figure S5, B and C) and make large fusion proteins that
651 approximate the predicted sizes of the GFP::ETC-1 fusion proteins (~150 kDa, see below)
652 (Figure 6E, lanes 1 and 2). We conclude that a start codon immediately adjacent to the *etc-1* 5'
653 trans-splice site is capable of initiating translation *in vivo*.

654 *etc-1(tn1919)* and *etc-1(tn1920)* express GFP::ETC-1 (labeled GFP_F::ETC-1) in the
655 oogenic germline of hermaphrodites, where it is both cytoplasmic and nucleoplasmic (Figure 6,
656 C and D). We observed no significant difference in the amount of cytoplasmic GFP::ETC-1 in
657 the germlines of *etc-1(tn1919)* (n=11) and *etc-1(tn1920)* (n=8) adult hermaphrodites (P>0.1
658 using a Student's *t*-test). In addition, both alleles express GFP::ETC-1 in embryos (Figure 6, C
659 and D) and in a variety of somatic tissues, including the intestine, the spermatheca, and
660 unidentified cells near the pharynx (arrow in Figure S5, B and C). Interestingly, *etc-1(tn1920)*
661 adult hermaphrodites (n=3) express 2.4-fold more GFP::ETC-1 in the unidentified cells near the
662 pharynx than *etc-1(tn1919)* adult hermaphrodites (n=7) ($P<1x10^{-6}$ using a Student's *t*-test). This

663 result suggests there could be differential start codon usage in some cell types. In *etc-1(tn1920)*
664 animals, the start codon at the beginning of the GFP coding sequence is 60 bp downstream of
665 ATG #1 and in the same relative position as the annotated start codon (ATG #2) in the
666 endogenous *etc-1* gene (Figure S5A). We hypothesized that *etc-1(tn1920)* animals might be able
667 to initiate GFP::ETC-1 translation both at the start codon used by *etc-1(tn1919)* animals (150.5
668 kDa GFP::ETC-1) and at the start codon located at the beginning of the GFP coding sequence
669 (148 kDa GFP::ETC-1). Consistent with this idea, some of the GFP::ETC-1 made by *etc-*
670 *1(tn1920)* animals appears to migrate slightly faster on western blots (Figure 6E, lane 2). These
671 observations suggest that ETC-1 translation can initiate at ATG #1 in most tissues, including the
672 germline, while leaving the possibility that ETC-1 translation also initiates at ATG #2 in some
673 somatic cells. However, it is also possible that the slightly different GFP expression patterns seen
674 in *etc-1(tn1919)* and *etc-1(tn1920)* are caused by a difference in gene structure that we have not
675 explicitly considered or the fact that these alleles are differently functional. As we will describe,
676 *etc-1(tn1919)* (ATG #1) appears to be largely functional during the OET, while *etc-1(tn1920)*
677 (ATG #2) resembles the strong loss-of-function *etc-1(gk5182)* allele.

678

679 ***ETC-1 is non-essential***

680 *etc-1(RNAi)* and *etc-1(tm5615)* deletion animals are viable and fertile; they do not have an overt
681 phenotype in an otherwise wild-type background (Wang *et al.* 2013). Whereas *etc-1(tm5615)* is
682 predicted to be an in-frame deletion (Figure 6A), *etc-1(gk5182)* is a premature stop codon in the
683 second exon of the *etc-1* gene (Figure 6A). This suggested to us that *etc-1(gk5182)* should be a
684 strong loss-of-function allele. We therefore examined these animals for a variety of phenotypes,

685 including fertility defects, but failed to find any obvious problems. For example, the brood size
686 of *etc-1(gk5182)* hermaphrodites was no different from that of the wild type at 20 ºC [285.0 ±
687 25.2 (n=23) for *etc-1(gk5182)* vs. 292.8 ± 20.7 (n=20) in the wild type; *P*= 0.2784, *t* test]. *etc-*
688 *1(gk5182)* hermaphrodites also exhibited only low levels of embryonic lethality [0.3 ± 0.3 %
689 embryonic lethality (n=6575) for *etc-1(gk5182)* vs. 0.2 ± 0.3 (n=5853) in the wild type]. We
690 tested whether the strong loss-of-function mutation *sel-10(ar41)* (Figure S1A) would provide a
691 sensitized background to reveal defects because SEL-10 and ETC-1 both help degrade proteins
692 during the first meiotic division. However, *etc-1(gk5182)*; *lon-3(e2175)* and *etc-1(gk5182)*; *lon-*
693 *3(e2175) sel-10(ar41)* hermaphrodites are essentially indistinguishable and produce large
694 numbers of progeny [286 ± 26 larvae (n=14) and 283 ± 29 larvae, (n=15), respectively, at 20 °C].
695 These brood sizes are similar to the brood sizes of *lon-3(e2175)* and *lon-3(e2175) sel-10(ar41)*
696 hermaphrodites at 20 °C (Spike *et al.* 2018). We examined whether *etc-1(gk5182)* animals are
697 unusually sensitive to elevated temperatures because Hul5, the ETC-1 ortholog of budding yeast,
698 facilitates the degradation of protein aggregates that form during heat stress (Fang *et al*. 2011).
699 However, *etc-1(gk5182)* animals are homozygous viable and fertile at 25 °C and can be
700 maintained at this temperature for multiple generations. When wild-type animals are heat-
701 stressed for 3 hours at 31 °C, partially penetrant embryonic lethality occurs in the 24-hour period
702 immediately after the stress is applied (Huelgas-Morales *et al.* 2016). Using this heat stress
703 protocol, similar percentages of embryos produced within the relevant 24-hour period died when
704 we compared animals with the *etc-1(gk5182)* genotype (21% lethality, n=565 embryos, n=12
705 animals) to the wild type (26% lethality, n=463 embryos, n=11 animals). Wild-type L4-stage
706 larvae shifted from 20 °C to 37 °C for 1.5 hours exhibit partially penetrant larval arrest and

707 lethality (Zevian and Yanowitz 2014). Using this protocol, similar percentages of wild-type
708 (54%, n=268) and *etc-1(gk5182)* mutant animals (48%, n=300) died after heat shock.

709 To unambiguously determine whether ETC-1 is important for fertility or viability, we
710 used CRISPR-Cas9 genome editing to generate the *etc-1(tn2077)* null allele, which deletes the
711 entire *etc-1* open reading frame (Figure 6A). *etc-1(tn2077)* mutants are viable and fertile at all
712 temperatures tested (15, 20, and 25°C), confirming that *etc-1* is a non-essential gene in *C.*
713 *elegan*s under standard laboratory conditions. Like *etc-1(gk5182)* hermaphrodites, *etc-1(tn2077)*
714 hermaphrodites exhibit negligible embryonic lethality [0.3 ± 0.6 % embryonic lethality
715 (n=4304)]. However, *etc-1(tn2077)* hermaphrodites produce significantly lower brood sizes than
716 *etc-1(gk5182)* hermaphrodites [178.8 ± 55.6 (n=24) for *etc-1(tn2077)* vs. 285.0 ± 25.2 (n=23) for
717 *etc-1(gk5182)*; $P < 0.0001$, *t* test]. We also observed that *etc-1(tn2077)* hermaphrodites were
718 sluggish and appeared to exhibit a reduced life span (D.G., unpublished results). The reduced
719 brood size of *etc-1(tn2077)* hermaphrodites might be due to the production of less sperm, which
720 is ordinarily limiting for fertility. Whether this speculation proves correct and reflects the role of
721 ubiquitin-mediated protein degradation in germline sex determination (Starostina *et al*. 2007),
722 will require further study. Although the differences between *etc-1(gk5182)* and the large *etc-*
723 *1(tn2077)* deletion could in principle be due to impacts on neighboring genes, these phenotypic
724 differences are consistent with the idea that *etc-1(gk5182)* possibly retains residual ETC-1
725 function.

726

727

728

729 ***etc-1 alleles exhibit a genetic interaction with the anaphase promoting complex***

730 Wang *et al.* (2013) reported that *etc-1(RNAi)* enhances the phenotype of *mat-1(ax161*ts*); him-*
731 *8(e1489)* animals at the permissive temperature, and causes them to produce one-cell arrested
732 embryos. This enhancement supported the idea that ETC-1 and the anaphase promoting complex
733 (APC) share redundant functions during the OET, including the degradation of the key cell cycle
734 regulators IFY-1/securin and CYB-1/Cyclin B. We initially revisited this genetic interaction
735 using *etc-1(gk5182)* and two different temperature-sensitive alleles that attenuate APC function
736 in *C. elegans*: *emb-30(tn377*ts*)* and *mat-1(ax161*ts*)* (Furuta *et al.* 2000, Shakes *et al.* 2003).
737 Contrary to expectation, we found that *etc-1(gk5182); emb-30(tn377*ts*)* and *mat-1(ax161*ts*); etc-*
738 *1(gk5182)* double mutants are each homozygous viable and fertile at 15 °C. To extend this result,
739 we examined the number of larvae produced by *mat-1(ax161*ts*); etc-1(gk5182)* and *mat-*
740 *1(ax161*ts*)* parents. These animals were initially derived from *mat-1*-balanced strains (Table S1).
741 For each strain, we counted the number of larvae produced by parents that were third-generation
742 *mat-1(ax161*ts*)* homozygotes raised at 15 °C. *mat-1(ax161*ts*); etc-1(gk5182)* animals produced
743 fewer progeny (100 ± 35 larvae, n=15 animals) than *mat-1(ax161*ts*)* animals (165 ± 46 larvae,
744 n=17 animals) and this difference is statistically significant (P=0.0001). However, we did not
745 observe that the *mat-1(ax161*ts*); etc-1(gk5182)* double mutants produced one-cell arrested
746 embryos. Thus, the double mutant phenotype is not comparable to the embryonic arrest
747 phenotype of *mat-1(ax161*ts*)* (Figure S6B) or *mat-1(ax161*ts*)*; *him-8(e1489)* animals at 25 °C
748 (Shakes *et al.* 2003).

749 Since our phenotypic analyses suggested that *etc-1(gk5182)* might retain some residual
750 function, we analyzed whether *etc-1(tn2077)* exhibits a stronger genetic interaction with *mat-*
751 *1(ax161*ts*)*. We observed that *mat-1(ax161*ts*); etc-1(tn2077)* hermaphrodites are viable and

752 fertile at 15°C and produce embryos that can undergo multiple rounds of cell division (Figure
753 S6C). Some of these embryos hatch and grow into larvae. However, *mat-1(ax161*ts*); etc-*
754 *1(tn2077)* hermaphrodites produce many fewer larvae than *mat-1(ax161*ts*); etc-1(gk5182)*
755 hermaphrodites at 15 ºC. First-generation homozygotes derived from *mat-1(ax161*ts)/*tmC18*; *etc-*
756 *1(tn2077)* parents produced, on average, 28 ± 19 larvae (n=18). Second-generation homozygotes
757 were also fertile and produced a similarly small number of larvae [24 ± 14 larvae (n=36)].
758 However, dead embryos were also observed among the progeny of *mat-1(ax161*ts*); etc-*
759 *1(tn2077)* hermaphrodites, and dead embryos were typically more common than hatched larvae
760 when both of these were counted (n=12 of 18 second-generation egg lays). Although we did not
761 observe the one-cell arrest phenotype or the oocyte defects that were previously described
762 (Figure S6), these observations nonetheless confirm that *mat-1(ax161*ts*)* embryonic lethality is
763 enhanced by *etc-1(tn2077)*, albeit at a later stage of embryogenesis that may result from a defect
764 in mitotic cell division.

765

766 ***GFP-fusion proteins are partially proteolyzed in etc-1(gk5182) animals***

767 The PUF-3::GFP, PUF-11::GFP, CYB-1::GFP and IFY-1::GFP fusion proteins each contain
768 three FLAG epitope tags in addition to the fluorescent protein tag (Figure S1C, Sarov *et al.*
769 2012). We used an antibody that recognizes the FLAG tag to examine each fusion protein by
770 western blot in wild-type and *etc-1(gk5182)* hermaphrodites. Full-length PUF-3::GFP, PUF-
771 11::GFP and CYB-1::GFP fusion proteins migrate as expected in lysates made from both wild-
772 type and *etc-1(gk5182)* hermaphrodites (Figure 7A, lanes 1–6), while the IFY-1::GFP fusion
773 protein migrates slightly slower than expected (Figure 7C, lanes 1 and 2). However, in each *etc-*

774 *1(gk5182)* lysate, a second band is also recognized by the anti-FLAG antibody (Figure 7A, lanes
775 2, 4, and 6, and Figure 7C, lane 2). This *etc-1(gk5182)*-specific band only accumulates when a
776 GFP fusion protein is present (Figure S7A, compare lanes 2–7 with lanes 1 and 8) and can be
777 recognized by a GFP-specific antibody (Figure S7B, lanes 2, 4, and 6). Depending on the GFP
778 fusion protein, it migrates slightly faster (Figure 7A, lanes 2, 4, and 6) or slower (Figure 7C, lane
779 2) than a 40 kDa molecular weight marker. But in each case, the *etc-1(gk5182)*-specific band is
780 predicted, based on size, to encompass the entire 31–32 kDa GFP::FLAG tag (File S2). We
781 estimate that these GFP::FLAG fragments account for 10–20% of the total signal in each *etc-*
782 *1(gk5182); puf-3(tn1820[puf-3::gfp::3xflag])* lane, 4–11% of the total signal in each *etc-*
783 *1(gk5182); puf-11(tn1824[puf-11::gfp::3xflag)* lane and 4–10% of the total signal in each *etc-*
784 *1(gk5182); cyb-1(tn1806[cyb-1::gfp::3xflag])* lane (Figure 7A, lanes 2, 4, and 6). GFP::FLAG
785 fragments appear to be less abundant in *etc-1(gk5182); ddIs128[ify-1::gfp::3xflag]* animals
786 relative to the full length IFY-1::GFP fusion protein (Figure 7C), but we could not make an
787 accurate assessment of this difference because the full-length fusion protein and fragment were
788 not in the linear range of detection at the same time. These observations suggest that the GFP
789 fluorescence observed in *etc-1(gk5182)* embryos (Figure 5, A–D and G–J) may derive from
790 GFP::FLAG fragments rather than full-length PUF-3::GFP, PUF-11::GFP, CYB-1::GFP, or IFY-
791 1::GFP fusion proteins.

792 Our observations of GFP fluorescence in living *etc-1(lf)* animals suggest that *etc-*
793 *1(gk5182)* perturbs protein degradation during the OET (Figure 5). However, if the GFP::FLAG
794 fragments generated from each fusion protein accumulate prior to this time (during oogenesis,
795 for example), they might simply become easier to visualize when the full-length fusion protein is
796 degraded during the OET. We examined whether GFP::FLAG fragments are generated from the

797 PUF-3::GFP, PUF-11::GFP and CYB-1::GFP fusion proteins in unmated *etc-1(gk5182); fog-*
798 *2(oz40)* females to address this possibility. Development of the oogenic germline is normal in
799 *fog-2* mutant females, but due to the absence of the major sperm protein signal from sperm
800 (McCarter *et al.* 1999; Miller *et al.* 2001), the rate of oocyte meiotic maturation is substantially
801 decreased, and fertilization and embryo formation are prevented. We found that GFP::FLAG
802 fragments are generated from each fusion protein in *etc-1(gk5182); fog-2* females (Figure 7B,
803 lanes 2, 4, and 6; see Figure S7D for a longer exposure). Relative to the amount of each full-
804 length fusion protein, however, GFP::FLAG fragments appear to be considerably less abundant
805 in unmated *etc-1(gk5182); fog-2* females than in *etc-1(gk5182)* hermaphrodites (compare Figure
806 7, A and B) or mated *etc-1(gk5182); fog-2* females (compare Figure 7B and Figure S7, C and D).
807 This was most noticeable for the GFP::FLAG fragments derived from CYB-1::GFP and PUF-
808 11::GFP. These observations suggest that many of the GFP::FLAG fragments produced by *etc-*
809 *1(gk5182)* mutant hermaphrodites and mated females are generated when each GFP fusion
810 protein is degraded during the OET.

811 GFP::FLAG fragments also accumulate in *etc-1(gk5182); cyb-1(tn1806); fog-2(oz40)*
812 adult males (Figure 7B, lane 8). Endogenous CYB-1 is abundant in the male germline and
813 eliminated toward the end of meiosis (Yoon *et al.* 2017). CYB-1::GFP exhibits a similar pattern
814 of accumulation in *fog-2* males (Figure S8, A and B). In *etc-1(gk5182); fog-2* males, however, a
815 GFP signal perdures past the stage where CYB-1::GFP is normally eliminated (Figure S8, C and
816 D). Much of this signal localizes to residual bodies (Figure S8, E and F). Residual bodies form at
817 the end of the second meiotic division and receive cellular materials that are not required during
818 subsequent stages of spermatogenesis (Ward *et al.* 1981; reviewed in Chu and Shakes 2013). It
819 seems likely that, as in *etc-1(gk5182)* embryos, the GFP fluorescence seen in *etc-1(gk5182)*

820 residual bodies derives from GFP::FLAG fragments that are formed when CYB-1::GFP is
821 degraded during male meiosis.

822

823 ***ETC-1 may promote proteasome processivity***

824 Hul5 and UBE3C, the yeast and human orthologs of ETC-1, are proteasome-associated ubiquitin
825 ligases that help the proteasome degrade difficult substrates (Crosas *et al.* 2006; Fang *et al.* 2011;
826 Kuo and Goldberg 2017; Gottlieb *et al.* 2019). In this context, Hul5 and UBE3C are thought to
827 be important for the processive degradation of proteins that are stalled on the proteasome. This
828 hypothesis was based, in part, on experiments with GFP fusion proteins. In the absence of Hul5,
829 or after UBE3C knockdown, the proteasomal degradation of substrates consisting of an unstable
830 domain fused with the much more stable GFP domain is incomplete. This results in the
831 accumulation of stable GFP-containing fragments of the original fusion protein (Aviram and
832 Kornitzer 2010; Martinez-Noël *et al.* 2012; Chu *et al.* 2013). The experiments described in the
833 previous section strongly suggest that ETC-1 plays a similar role in *C. elegans*. We added to
834 these observations by examining additional GFP and non-GFP-tagged fusion proteins in *etc-1(lf)*
835 hermaphrodites, as described below.

836 ***GFP::ETC-1 fusion proteins:*** Neither GFP::ETC-1 fusion protein is partially processed to a
837 substantial extent (Figure 6E, lanes 1 and 2). To determine whether either GFP-tagged allele is
838 functional *in vivo*, we examined whether PUF-3::GFP is partially processed in *etc-1(tn1919)* and
839 *etc-1(tn1920)* hermaphrodites. GFP::FLAG fragments accumulate in PUF-3::GFP-expressing
840 *etc-1(tn1920)* animals (Figure 6E, lane 6) and are similar in abundance to the GFP::FLAG
841 fragments seen in *etc-1(gk5182)* animals (Figure 6E, lane 4). *etc-1(tn1920)* therefore appears to

842 be a strong loss-of-function mutation. Only a very small amount of the PUF-3::GFP-derived
843 GFP::FLAG fragment accumulates in *etc-1(tn1919)* animals (Figure 6E, see the longer exposure
844 of lane 5), suggesting that *etc-1(tn1919)* retains a significant amount of function in the *C.*
845 *elegans* germline. It is not clear why GFP::ETC-1-derived GFP::FLAG fragments do not
846 substantially accumulate in *etc-1(tn1920)* animals. Possibly ETC-1 itself is not a substrate for
847 proteasomal degradation. Alternatively, it is possible that these fragments accumulate to a level
848 that is below our detection threshold. In this regard, it is worth noting that GFP::ETC-1 is
849 expressed at much lower levels than PUF-3::GFP (Figure 6E).

850 ***RNP-8::GFP fusion proteins:*** We created a GFP-tagged allele of *rnp-8* (Figure S1C; RNP-
851 8::GFP_F in all figures) and found that RNP-8::GFP is abundantly expressed in oocytes and early
852 embryos (Figure S9A). We do not know whether this GFP-tagged allele of *rnp-8* (*rnp-*
853 *8(tn1860[rnp-8::gfp:3xflag])*) is functional *in vivo*. Although RNP-8 is thought to be degraded in
854 response to oocyte maturation (Kim *et al*. 2010), RNP-8::GFP is not strongly down-regulated
855 during the oocyte-to-embryo transition (Figure S9A). GFP fluorescence is not obviously
856 increased in *rnp-8(tn1860*); *etc-1(gk5182)* animals compared to *etc-1(+)* control animals (Figure
857 S9, A and B). Nevertheless, a small proportion of the RNP-8::GFP fusion protein made by *rnp-*
858 *8(tn1860*) is partially processed into GFP::FLAG fragments in *etc-1(gk5182)* hermaphrodites
859 (Figure S7C, lanes 7 and 8); however, this might represent a low level of turnover at other stages
860 of germline development distinct from the OET.

861 ***LIN-41 fusion proteins:*** Only full-length mSCARLET::LIN-41 fusion proteins accumulate to a
862 substantial level in wild-type, *etc-1(gk5182)* and *sel-10(lf)* hermaphrodites (Figure 7D). We did
863 not detect mSCARLET::FLAG or DENDRA::FLAG fragments at elevated levels in *etc-*
864 *1(gk5182)*, *sel-10(ar41)* or *sel-10(ok1632)* animals (Figure 7D; Figure S7E). This is consistent

865 with the observation that the levels of fluorescence appear to be the same in embryos made by
866 wild-type and *etc-1(gk5182)* animals that express mSCARLET::LIN-41 (Figure 5, E and F) and
867 the conclusion that the *etc-1(gk5182)* mutation does not perturb the SEL-10-mediated
868 degradation of mSCARLET::LIN-41 or DENDRA::LIN-41 that we documented using
869 fluorescence microscopy (Figure 1, A and B; Figure 2). We tested whether GFP::LIN-41 would
870 behave in the same way by crossing our original GFP-tagged *lin-41(tn1541)* allele (Figure S1B;
871 GFP_S::LIN-41 below and in all figures) into an *etc-1(gk5182)* genetic background. However, we
872 found that GFP is not appropriately down-regulated in the embryos of *lin-41(tn1541)*; *etc-*
873 *1(gk5182)* hermaphrodites compared to *lin-41(tn1541)*; *etc-1(+)* controls (Figure S9, C and D).
874 These observations suggest that GFP_S::LIN-41 is partially processed in *etc-1(gk5182)*
875 hermaphrodites and imply that GFP-tagged fusion proteins might be more recalcitrant than other
876 fusion proteins to processivity-challenged proteasomes.

877 To rigorously investigate these possibilities, we created new *lin-41* alleles that express a
878 GFP::FLAG-tagged LIN-41 fusion protein (GFP_F::LIN-41). We isolated two independent
879 insertions that were given different allele names [*lin-41(tn2054[gfp::3xflag::lin-41])* and *lin-*
880 *41(tn2055[gfp::3xflag::lin-41])*, see Figure S1B]; these two alleles are molecularly identical and
881 were used interchangeably in our experiments. Interestingly, GFP fluorescence in GFP_F::LIN-41-
882 expressing worms is much brighter than in GFP_S::LIN-41-expressing worms (compare Figures
883 S8, E and G), possibly because the mRNA sequence that encodes the GFP::3xFLAG tag has a
884 much higher codon adaptation index (CAI=0.92) than the sequence that encodes the GFP::S tag
885 (CAI=0.28) (Redemann *et al*. 2011). More than half of the GFP_F::LIN-41-expressing animals
886 also exhibit a defect in egg laying (Egl phenotype) as adult hermaphrodites at 20°C (Figure
887 S9H). A similar phenotype is observed when LIN-41 is over-expressed in somatic cells during

888 the fourth larval (L4) stage by interfering with *let-7* microRNA regulation (e.g., using the *lin-*
889 *41(xe11*gf*)* allele described by Ecsedi *et al.* 2015). With respect to our tagged alleles of *lin-41*,
890 however, this defect uniquely characterizes the GFP::FLAG tagged alleles, as most GFP_S::LIN-
891 41 (Figure S9F), mSCARLET::LIN-41, and DENDRA::LIN-41-expressing adults do not have an
892 Egl phenotype. Despite these intriguing differences, the temporal expression pattern and
893 regulation of GFP_F::LIN-41 strongly resembles GFP_S::LIN-41. Most importantly, GFP_F::LIN-41-
894 expressing animals exhibit higher levels of GFP fluorescence in the early embryos made by *sel-*
895 *10(ok1632)* and *etc-1(gk5182)* mutants relative to otherwise wild-type hermaphrodites (Figure 5,
896 K and L; Figure S9, I–N). Interestingly, the subcellular localization pattern of GFP_F::LIN-41-
897 derived GFP fluorescence is distinctly different in the early embryos made by *sel-10(ok1632)*
898 and *etc-1(gk5182)* mutant hermaphrodites (Figure S9, K and M). In *sel-10(ok1632)* embryos,
899 GFP fluorescence is primarily cytoplasmic and appears to be enriched in ribonucleoprotein
900 particles called P granules (Figure S9M). Localization to embryonic P granules is also observed
901 when LIN-41 degron sequences are disrupted in GFP_S::LIN-41 (Spike *et al.* 2018). In *etc-*
902 *1(gk5182)* embryos, however, GFP fluorescence does not localize to P granules and is slightly
903 enriched in the nucleus (Figure S9K). These observations are consistent with the idea that
904 GFP_F::LIN-41 is partially processed into a GFP-containing protein fragment that is largely
905 responsible for the excess fluorescence observed in early *etc-1(gk5182)* embryos.

906 The only difference between GFP_F:::LIN-41, mSCARLET::LIN-41 and DENDRA::LIN-
907 41 is the fluorescent protein fused to LIN-41 (Figure S1B). We examined all of these proteins in
908 *etc-1(gk5182)* and *etc-1(+)* hermaphrodites by western blot, and confirmed that GFP::FLAG
909 fragments accumulate in GFP_F:::LIN-41-expressing *etc-1(gk5182)* adults at elevated levels
910 relative to *etc-1(+)* animals (Figure 7E). A longer exposure of the same western blot revealed

911 low levels of GFP::FLAG fragments even in *etc-1(+)* hermaphrodites (Figure S7F, lane 5).
912 However, *etc-1*-dependent fragments derived from the mSCARLET::LIN-41 and
913 DENDRA::LIN-41 fusion proteins were not observed. We conclude that *etc-1(gk5182)*
914 specifically disrupts the proteolysis of the GFP-containing LIN-41 fusion proteins (GFP_F::LIN-
915 41 and GFP_S::LIN-41) and speculate that tagging LIN-41 with GFP creates a LIN-41 fusion
916 protein that is more difficult to degrade. Consistent with this idea, GFP is known to be a
917 particularly stable fluorescent protein that can be difficult for the proteasome to degrade
918 (Khmelinskii *et al.* 2016; Reichard *et al.* 2016; Bragança and Kraut 2020). Based on these
919 observations, we propose that fusion with GFP is an important cause of the proteolysis defects
920 observed in *etc-1(gk5182)* animals (Figures 5 and 7). In this context, we note the study that
921 identified and described ETC-1 as a target-specific E3 ubiquitin ligase in *C. elegans* (Wang *et al.*
922 2013) relied on GFP fusion proteins and monitored protein degradation by looking exclusively at
923 fluorescence. Our observations suggest, instead, that the *C. elegans etc-1* gene has the same type
924 of activity described for orthologous genes in yeast and humans (Aviram and Kornitzer 2010;
925 Martinez-Noël *et al.* 2012; Chu *et al.* 2013) and that the ETC-1 protein promotes proteasome
926 processivity, which may be especially important during the OET when many proteins are
927 targeted for efficient proteasomal degradation.

928

929 **DISCUSSION**

930 ***Proteolysis and translational repression limit the expression of RNA-binding proteins during***
931 ***the OET***

932 Many of the oocyte-expressed proteins degraded during the OET in *C. elegans* are RNA-binding
933 proteins that regulate translation (reviewed by Robertson and Lin 2013, 2015). These RNA-
934 binding proteins include LIN-41 and the Pumilio/FBF-family RNA-binding proteins PUF-3 and
935 PUF-11. PUF-3 and PUF-11 function redundantly, repress the translation of specific targets in
936 oocytes, and play important roles in germline stem cells and embryonic development in *C.*
937 *elegans* (Hubstenberger *et al.* 2012; Haupt *et al.* 2020). Since PUF-3 and PUF-11 appear to be
938 degraded soon after meiotic maturation (Figure 3), it seems likely that the maternal-effect
939 embryonic lethality caused by an absence of both proteins is due to mRNA translation defects in
940 developing oocytes. Interestingly, the timing and regulation of PUF-3 and PUF-11 degradation
941 appear to be temporally and molecularly coordinated with meiotic maturation and strongly
942 resemble what we have described for LIN-41 (Spike *et al.* 2018 and Figure 3). The resemblances
943 include a requirement for active CDK-1 (Figure 4), which is essential for entry into meiotic M-
944 phase (Boxem *et al.* 1999, Burrows *et al.* 2006), and independence from APC ubiquitin ligase
945 subunits that promote the subsequent metaphase-to-anaphase transition (Furuta *et al.* 2000;
946 Shakes *et al.* 2003). Additional connections between LIN-41, PUF-3, and PUF-11 include the
947 identification of each protein and mRNA in purified LIN-41 RNPs, and the identification of
948 LIN-41 and PUF-3/11 as factors important for the 3'UTR-mediated translational repression of a
949 common target, the Rbfox-related RNA-binding protein SPN-4 (Hubstenberger *et al.* 2012;
950 Tsukamoto *et al*. 2017). These disparate observations suggest that LIN-41, PUF-3, and PUF-11
951 might collaborate and function, at least in part, as components of a regulatory RNP to inhibit the
952 translation of SPN-4 in developing oocytes. Previously, we proposed that LIN-41 is inactivated

953 as a translational repressor prior to its degradation (Spike *et al*. 2018). Since *cdk-1(RNAi)* does
954 not reduce or eliminate SPN-4::GFP expression in early embryos (Tsukamoto *et al.* 2017), we
955 speculate that PUF-3 and PUF-11 are likewise inactivated prior to their degradation. Thus, we
956 suggest that the function of a LIN-41/PUF-3/PUF-11 RNP is down-regulated through both CDK-
957 1-dependent and -independent mechanisms near the end of oogenesis.

958

959 ***ETC-1, the APC, and proteasome processivity during the OET***

960 Wang *et al.* (2013) identified and described ETC-1 (UB*E* *T*hree *C*), the *C. elegans* UBE3C
961 ortholog, as a HECT-type E3 ubiquitin ligase that promotes the degradation of the essential cell
962 cycle proteins IFY-1/Securin and CYB-1/Cyclin B1 during the OET. Degradation was monitored
963 using a GFP fusion protein (IFY-1::GFP or GFP::CYB-1), immunoprecipitation assays clearly
964 documented a specific interaction between the GFP fusion protein and ETC-1, and *in vitro*
965 assays confirmed that ETC-1 is able to interact with, and ubiquitylate, each target protein. These
966 findings were consistent at the time with the interpretation that ETC-1 functions as an E3
967 ubiquitin ligase. However, they are also compatible with our results that suggest instead that
968 ETC-1 functions as an E4 enzyme that mediates ubiquitin chain elongation for the processive
969 degradation of proteins already targeted for ubiquitin conjugation by E3 enzymes—a function
970 shown for Hul5 in budding yeast (Crosas *et al*. 2006). When combined with the observation that
971 *etc-1(RNAi)* enhanced the one-cell arrest phenotype of mutants with a compromised APC (e.g.,
972 *mat-1(ax161*ts*)*), the biochemical and cell biological observations of Wang *et al*. (2013) appeared
973 to support a simple and sensible model: that ETC-1 and the anaphase promoting complex target
974 the same *C. elegans* proteins (e.g., IFY-1 and CYB-1) for ubiquitination and degradation during

975 the OET. We revisited the genetic interaction between *etc-1* and the anaphase promoting
976 complex, at least in part, because our new results suggest that ETC-1 is not a substrate-specific
977 E3 ligase and make it seem unlikely that ETC-1 plays a prominent role in the degradation of
978 endogenous IFY-1 or CYB-1. Rather, our findings suggest that *etc-1* mutants have difficulty
979 degrading GFP-fusion proteins. The fact that *etc-1(tn2077)* null and *etc-1(gk5182)* loss-of-
980 function mutants exhibit minimal embryonic lethality is consistent with this idea. Using *etc-*
981 *1(tn2077)*, a molecular null mutation that deletes the entire *etc-1* open reading frame, we
982 confirmed that the embryo lethal phenotype of *mat-1(ax161*ts*)* is substantially enhanced at 15 ºC
983 in the absence of ETC-1. However, because the embryos produced by *mat-1(ax161ts); etc-*
984 *1(tn2077)* hermaphrodites are primarily multicellular, this genetic interaction may reflect a defect
985 in mitotic cell division rather than a defect in the OET.

986

987 ***The in vivo dynamics of GFP-fusion protein degradation in the absence of ETC-1***

988 Our analyses of several different GFP fusion proteins, including GFP fusions with IFY-1 and
989 CYB-1, provide a clear explanation for the apparent perdurance of each protein in the absence of
990 ETC-1. It appears that the addition of a GFP moiety to several proteins that are rapidly degraded
991 during the OET, such as IFY-1, CYB-1, PUF-3, PUF-11, or LIN-41, creates fusion proteins that
992 are incompletely degraded in the absence of *etc-1* function. Incomplete degradation results in the
993 accumulation of a partial GFP-containing fragment in embryos that is easily confused for the
994 full-length GFP fusion protein when only fluorescence is examined. Evidence that the GFP
995 moiety is a determining factor is derived from the analysis of LIN-41 fusion proteins. LIN-41
996 fusion proteins containing one of three different fluorescent proteins, mSCARLET, DENDRA or

997 GFP, were examined and the only fusion protein that was incompletely degraded in an ETC-1-
998 dependent manner was GFP::LIN-41 (Figure 7E). Our experiments do not demonstrate, however,
999 that the fused portion of the *C. elegans* protein is unimportant for determining whether substrate
1000 processivity is substantively reduced in the absence of ETC-1. For example, the GFP::ETC-1
1001 fusion protein made by the loss-of-function *etc-1(tn1920)* allele may not be partially processed
1002 (Figure 6E). Although it is tempting to speculate that this is because GFP::ETC-1 is not unstable
1003 during the OET (Figure 6D), some of our other experiments indicate that fragments can be
1004 generated even when proteins appear to be relatively stable. For example, RNP-8::GFP is
1005 partially processed to a small extent in *etc-1* mutants even though it is not rapidly degraded
1006 during the OET (Figures S6C and S8B). Likewise, the behaviors of PUF-3::GFP, PUF-11::GFP
1007 and CYB-1::GFP in unmated females (Figure 7B) argue for a more nuanced view. It seems likely
1008 that the proteasome helps degrade or "turn over" each GFP fusion protein to some extent in the
1009 adult germlines of unmated females and hermaphrodites. However, because each GFP-tagged
1010 protein is relatively stable prior to the OET, many fewer fragments are formed in females in the
1011 absence of *etc-1* function. We suggest that the properties conferred by each fused *C. elegans*
1012 protein likely explain why some GFP fusion proteins appear to be less sensitive to *etc-1* function
1013 than others, even when both proteins are rapidly degraded during the OET (e.g.: IFY-1::GFP and
1014 PUF-3::GFP in Figures 5 and 7). Consistent with this idea, sequences outside the GFP moiety
1015 have been shown to be important for the Hul5-dependent proteolytic processing of a GFP-Pcl5
1016 fusion protein in *S. cerevisiae* (Aviram and Kornitzer 2010), and it is becoming increasingly
1017 clear that the method and type of substrate ubiquitination influences proteasome processivity
1018 (Reichard *et al*. 2016; Bragança and Kraut 2020).

1019

1020 ***Conclusion***

1021 Our analysis of ETC-1 updates the literature to show that it plays a conserved role to promote
1022 proteasome processivity. Proteasome processivity may be critically important during the OET
1023 when many oocyte regulatory proteins are rapidly turned over. Our experiments also provide a
1024 cautionary note on the need to analyze endogenous proteins where possible, utilize multiple
1025 protein tags and, ideally, analyze proteins on western blots when studying protein degradation *in*
1026 *vivo*. Fortunately, the ease and rapidity of genome editing continues to revolutionize the ability to
1027 conduct such experiments in the *C. elegans* system (reviewed by Nance and Frøkjaer-Jensen
1028 2019).

1029 **ACKNOWLEDGMENTS**

1030 We thank the two anonymous reviewers for constructive suggestions, including the suggestion
1031 that we analyze an *etc-1* molecular null mutation. We are grateful to Bob Goldstein, Judith
1032 Kimble, Geraldine Seydoux, and Marcus Vargas for providing strains or reagents. Some strains
1033 were provided by the Caenorhabditis Genetics Center, which is funded by grant P40OD010440
1034 from the NIH Office of Research Infrastructure Programs. We also thank WormBase for
1035 sequences and annotations. Gabriela Huelgas-Morales and Todd Starich provided helpful
1036 suggestions during the course of this work. This work was supported by NIH grant GM144029
1037 (to D.G.).

1038

1039 **LITERATURE CITED**

1040 Allen, A. K., J. E. Nesmith, and A. Golden, 2014 An RNAi-based suppressor screen identifies
1041 interactors of the Myt1 ortholog of *Caenorhabditis elegans*. G3 (Bethesda) 4: 2329–
1042 2343.

1043 Allen, M. A., L. W. Hillier, R. H. Waterston, and T. Blumenthal, 2011 A global analysis of *C.*
1044 *elegans* trans-splicing. Genome Res 21: 255–264.

1045 Arribere, J. A., R. T. Bell, B. X. Fu, K. L. Artiles, P. S. Hartman *et al.*, 2014 Efficient marker-
1046 free recovery of custom genetic modifications with CRISPR/Cas9 in *Caenorhabditis*
1047 *elegans*. Genetics 198: 837–846.

1048 Aviram, S., and D. Kornitzer, 2010 The ubiquitin ligase Hul5 promotes proteasomal
1049 processivity. Mol Cell Biol 30: 985–994.

1050 Bachvarova, R., E. H. Davidson, V. G. Allfrey, and A. E. Mirsky, 1966 Activation of RNA
1051 synthesis associated with gastrulation. Proc Natl Acad Sci U S A 55: 358–365.

1052 Blitz, I. L., and K. W. Y. Cho, 2021 Control of zygotic genome activation in *Xenopus*. Curr Top
1053 Dev Biol 145: 167–204.

1054 Boxem, M., D. G. Srinivasan, and S. van den Heuvel, 1999 The *Caenorhabditis elegans* gene
1055 *ncc-1* encodes a cdc2-related kinase required for M phase in meiotic and mitotic cell
1056 divisions, but not for S phase. Development 126: 2227–2239.

1057 Bragança, C. E., and D. A. Kraut, 2020 Mode of targeting to the proteasome determines GFP
1058 fate. J Biol Chem 295: 15892–15901.

1059 Burrows, A. E., B. K. Sceurman, M. E. Kosinski, C. T. Richie, P. L. Sadler *et al.*, 2006 The *C.*
1060 *elegans* Myt1 ortholog is required for the proper timing of oocyte maturation.
1061 Development 133: 697–709.

1062 Cao, W. X., A. Karaiskakis, S. Lin, S. Angers, and H. D. Lipshitz, 2022 The F-box protein Bard
1063 (CG14317) targets the Smaug RNA-binding protein for destruction during the
1064 *Drosophila* maternal-to-zygotic transition. Genetics 220: iyab177.
1065 Cao, W. X., S. Kabelitz, M. Gupta, E. Yeung, S. Lin *et al.*, 2020 Precise temporal regulation of
1066 post-transcriptional repressors is required for an orderly *Drosophila* maternal-to-zygotic
1067 transition. Cell Rep 31: 107783.
1068 Chang, H. M., N. J. Martinez, J. E. Thornton, J. P. Hagan, K. D. Nguyen *et al.*, 2012 Trim71
1069 cooperates with microRNAs to repress Cdkn1a expression and promote embryonic stem
1070 cell proliferation. Nat Commun 3: 923.
1071 Chen, J., F. Lai, and L. Niswander, 2012 The ubiquitin ligase mLin41 temporally promotes
1072 neural progenitor cell maintenance through FGF signaling. Genes Dev 26: 803–815.
1073 Choi, W. J., M. W. Clark, J. X. Chen, and A. Y. Jong, 1990 The CDC4 gene product is
1074 associated with the yeast nuclear skeleton. Biochem Biophys Res Commun 172: 1324–
1075 1330.
1076 Chu, B. W., K. M. Kovary, J. Guillaume, L. C. Chen, M. N. Teruel *et al.*, 2013 The E3 ubiquitin
1077 ligase UBE3C enhances proteasome processivity by ubiquitinating partially proteolyzed
1078 substrates. J Biol Chem 288: 34575–34587.
1079 Chu, D. S., and D. C. Shakes, 2013 Spermatogenesis. Adv Exp Med Biol 757: 171–203.
1080 Chudakov, D. M., S. Lukyanov, and K. A. Lukyanov, 2007 Using photoactivatable fluorescent
1081 protein Dendra2 to track protein movement. Biotechniques 42: 553–563.
1082 Clegg, K. B., and L. Pikó, 1982 RNA synthesis and cytoplasmic polyadenylation in the one-cell
1083 mouse embryo. Nature 295: 343–344.
1084 Collins, G. A., and A. L. Goldberg, 2017 The logic of the 26S proteasome. Cell 169: 792–806.

1085 Crosas, B., J. Hanna, D. S. Kirkpatrick, D. P. Zhang, Y. Tone *et al.*, 2006 Ubiquitin chains are
1086 remodeled at the proteasome by opposing ubiquitin ligase and deubiquitinating activities.
1087 Cell 127: 1401–1413.
1088 Cuevas, E., A. Rybak-Wolf, A. M. Rohde, D. T. Nguyen, and F. G. Wulczyn, 2015
1089 Lin41/Trim71 is essential for mouse development and specifically expressed in postnatal
1090 ependymal cells of the brain. Front Cell Dev Biol 3: 20.
1091 Davis, P., M. Zarowiecki, V. Arnaboldi, A. Becerra, S. *et a*l., 2022 WormBase in 2022-data,
1092 processes, and tools for analyzing *Caenorhabditis elegans*. Genetics in press.
1093 de la Cova, C. and I. Greenwald, 2012 SEL-10/Fbw7-dependent negative feedback regulation of
1094 LIN-45/Braf signaling in *C. elegans* via a conserved phosphodegron. Genes Dev 26:
1095 2524–2535.
1096 Dejima, K., S. Hori, S. Iwata, Y. Suehiro, S. Yoshina *et al.*, 2018 An aneuploidy-free and
1097 structurally defined balancer chromosome toolkit for *Caenorhabditis elegans*. Cell Rep
1098 22: 232–241.
1099 Deshaies, R. J., and J. E. Ferrell, 2001 Multisite phosphorylation and the countdown to S phase.
1100 Cell 107: 819–822.
1101 Dickinson, D. J., A. M. Pani, J. K. Heppert, C. D. Higgins, and B. Goldstein, 2015 Streamlined
1102 genome engineering with a self-excising drug selection cassette. Genetics 200: 1035–
1103 1049.
1104 Dikic, I., 2017 Proteasomal and autophagic degradation systems. Annu Rev Biochem 86: 193–
1105 224.
1106 Ding, M., D. Chao, G. Wang, and K. Shen, 2007 Spatial regulation of an E3 ubiquitin ligase
1107 directs selective synapse elimination. Science 317: 947–951.

1108 Dorfman, M., J. E. Gomes, S. O'Rourke, and B. Bowerman, 2009 Using RNA interference to
1109 identify specific modifiers of a temperature-sensitive, embryonic-lethal mutation in the
1110 *Caenorhabditis elegans* ubiquitin-like Nedd8 protein modification pathway E1-activating
1111 gene *rfl-1*. Genetics 182: 1035–1049.
1112 Ecsedi, M., M. Rausch, and H. Großhans, 2015 The *let-7* microRNA directs vulval development
1113 through a single target. Dev Cell 32: 335–344.
1114 Edgar, L. G., N. Wolf, and W. B. Wood, 1994 Early transcription in *Caenorhabditis elegans*
1115 embryos. Development 120: 443–451.
1116 Fang, N. N., A. H. Ng, V. Measday, and T. Mayor, 2011 Hul5 HECT ubiquitin ligase plays a
1117 major role in the ubiquitylation and turnover of cytosolic misfolded proteins. Nat Cell
1118 Biol 13: 1344–1352.
1119 Finley, D., 2009 Recognition and processing of ubiquitin-protein conjugates by the proteasome.
1120 Annu Rev Biochem 78: 477–513.
1121 Furey, C. G., J. Choi, S. C. Jin, X. Zeng, A. T. Timberlake *et al.*, 2018 De Novo mutation in
1122 genes regulating neural stem cell fate in human congenital hydrocephalus. Neuron 99:
1123 302–314.
1124 Furuta, T., S. Tuck, J. Kirchner, B. Koch, R. Auty *et al.*, 2000 EMB-30: an APC4 homologue
1125 required for metaphase-to-anaphase transitions during meiosis and mitosis in
1126 *Caenorhabditis elegans*. Mol Biol Cell 11: 1401–1419.
1127 Gallo, C. M., J. T. Wang, F. Motegi, and G. Seydoux, 2010 Cytoplasmic partitioning of P
1128 granule components is not required to specify the germline in *C. elegans*. Science 330:
1129 1685–1689.
1130 Gottlieb, C. D., A. C. S. Thompson, A. Ordureau, J. W. Harper, and R. R. Kopito, 2019 Acute

1131 unfolding of a single protein immediately stimulates recruitment of ubiquitin protein
1132 ligase E3C (UBE3C) to 26S proteasomes. J Biol Chem 294: 16511–16524.
1133 Govindan, J. A., H. Cheng, J. E. Harris, and D. Greenstein, 2006 $G\alpha_{o/i}$ and $G\alpha_s$ signaling
1134 function in parallel with the MSP/Eph receptor to control meiotic diapause in *C. elegans*.
1135 Curr Biol 16: 1257–1268.
1136 Green, R. A., A. Audhya, A. Pozniakovsky, A. Dammermann, H. Pemble *et al.*, 2008 Expression
1137 and imaging of fluorescent proteins in the *C. elegans* gonad and early embryo. Methods
1138 Cell Biol 85: 179–218.
1139 Griffin, E. E., D. J. Odde, and G. Seydoux, 2011 Regulation of the MEX-5 gradient by a
1140 spatially segregated kinase/phosphatase cycle. Cell 146: 955–968.
1141 Gurskaya, N. G., V. V. Verkhusha, A. S. Shcheglov, D. B. Staroverov, T. V. Chepurnykh *et al.*,
1142 2006 Engineering of a monomeric green-to-red photoactivatable fluorescent protein
1143 induced by blue light. Nat Biotechnol 24: 461–465.
1144 Hamatani, T., M. G. Carter, A. A. Sharov, and M. S. Ko, 2004 Dynamics of global gene
1145 expression changes during mouse preimplantation development. Dev Cell 6: 117–131.
1146 Harrison, M. M., and M. B. Eisen, 2015 Transcriptional activation of the zygotic genome in
1147 *Drosophila*. Curr Top Dev Biol 113: 85–112.
1148 Haupt, K. A., K. T. Law, A. L. Enright, C. R. Kanzler, H. Shin *et al.*, 2020 A PUF hub drives
1149 self-renewal in *Caenorhabditis elegans* germline stem cells. Genetics 214: 147–161.
1150 Herrera, R. A., K. Kiontke, and D. H. Fitch, 2016 Makorin ortholog LEP-2 regulates LIN-28
1151 stability to promote the juvenile-to-adult transition in *Caenorhabditis elegans*.
1152 Development 143: 799–809.
1153 Hubbard, E. J., G. Wu, J. Kitajewski, and I. Greenwald, 1997 *sel-10*, a negative regulator of *lin-*

1154 *12* activity in *Caenorhabditis elegans*, encodes a member of the CDC4 family of
1155 proteins. Genes Dev 11: 3182–3193.
1156 Hubstenberger, A., C. Cameron, R. Shtofman, S. Gutman, and T. C. Evans, 2012 A network of
1157 PUF proteins and Ras signaling promote mRNA repression and oogenesis in *C. elegans*.
1158 Dev Biol 366: 218–231.
1159 Huelgas-Morales, G., and D. Greenstein, 2018 Control of oocyte meiotic maturation in *C.*
1160 *elegans*. Semin Cell Dev Biol 84: 90–99.
1161 Huelgas-Morales, G., C. G. Silva-García, L. S. Salinas, D. Greenstein, and R. E. Navarro, 2016
1162 The stress granule RNA-binding protein TIAR-1 protects female germ cells from heat
1163 shock in *Caenorhabditis elegans*. G3 (Bethesda) 6: 1031–1047.
1164 Jan, E., C. K. Motzny, L. E. Graves, and E. B. Goodwin, 1999 The STAR protein, GLD-1, is a
1165 translational regulator of sexual identity in *Caenorhabditis elegans*. EMBO J 18: 258–
1166 269.
1167 Jin, S. C., W. Dong, A. J. Kundishora, S. Panchagnula, A. Moreno-De-Luca *et al.*, 2020 Exome
1168 sequencing implicates genetic disruption of prenatal neuro-gliogenesis in sporadic
1169 congenital hydrocephalus. Nat Med 26: 1754–1765.
1170 Kanamoto, T., K. Terada, H. Yoshikawa, and T. Furukawa, 2006 Cloning and regulation of the
1171 vertebrate homologue of *lin-41* that functions as a heterochronic gene in *Caenorhabditis*
1172 *elegans*. Dev Dyn 235: 1142–1149.
1173 Kelly, W. G., S. Xu, M. K. Montgomery, and A. Fire, 1997 Distinct requirements for somatic
1174 and germline expression of a generally expressed *Caernorhabditis elegans* gene.
1175 Genetics 146: 227–238.
1176 Khmelinskii, A., M. Meurer, C. T. Ho, B. Besenbeck, J. Füller *et al.*, 2016 Incomplete

1177 proteasomal degradation of green fluorescent proteins in the context of tandem
1178 fluorescent protein timers. Mol Biol Cell 27: 360–370.
1179 Kim, K. W., T. L. Wilson, and J. Kimble, 2010 GLD-2/RNP-8 cytoplasmic poly(A) polymerase
1180 is a broad-spectrum regulator of the oogenesis program. Proc Natl Acad Sci U S A 107:
1181 17445–17450.
1182 Kipreos, E. T., 2005 Ubiquitin-mediated pathways in *C. elegans*. WormBook: 1–24.
1183 Kisielnicka, E., R. Minasaki, and C. R. Eckmann, 2018 MAPK signaling couples SCF-mediated
1184 degradation of translational regulators to oocyte meiotic progression. Proc Natl Acad Sci
1185 U S A 115: E2772–E2781.
1186 Kitagawa, R., E. Law, L. Tang, and A. M. Rose, 2002 The Cdc20 homolog, FZY-1, and its
1187 interacting protein, IFY-1, are required for proper chromosome segregation in
1188 *Caenorhabditis elegans*. Curr Biol 12: 2118–2123.
1189 Kloosterman, W. P., E. Wienholds, R. F. Ketting, and R. H. Plasterk, 2004 Substrate
1190 requirements for *let-7* function in the developing zebrafish embryo. Nucleic Acids Res
1191 32: 6284–6291.
1192 Kotani, T., K. Maehata, and N. Takei, 2017 Regulation of translationally repressed mRNAs in
1193 zebrafish and mouse oocytes. Results Probl Cell Differ 63: 297–324.
1194 Kuo, C. L., and A. L. Goldberg, 2017 Ubiquitinated proteins promote the association of
1195 proteasomes with the deubiquitinating enzyme Usp14 and the ubiquitin ligase Ube3c.
1196 Proc Natl Acad Sci U S A 114: E3404–E3413.
1197 Lambert, T. J., 2019 FPbase: a community-editable fluorescent protein database. Nat Methods
1198 16: 277–278.
1199 Latham, K. E., J. I. Garrels, C. Chang, and D. Solter, 1991 Quantitative analysis of protein

1200 synthesis in mouse embryos. I. Extensive reprogramming at the one- and two-cell stages.
1201 Development 112: 921–932.
1202 Lau, N. C., L. P. Lim, E. G. Weinstein, and D. P. Bartel, 2001 An abundant class of tiny RNAs
1203 with probable regulatory roles in *Caenorhabditis elegans*. Science 294: 858–862.
1204 Lin, Y. C., L. C. Hsieh, M. W. Kuo, J. Yu, H. H. Kuo *et al.*, 2007 Human TRIM71 and its
1205 nematode homologue are targets of *let-7* microRNA and its zebrafish orthologue is
1206 essential for development. Mol Biol Evol 24: 2525–2534.
1207 Liu, J., S. Vasudevan, and E. T. Kipreos, 2004 CUL-2 and ZYG-11 promote meiotic anaphase II
1208 and the proper placement of the anterior-posterior axis in *C. elegans*. Development 131:
1209 3513–3525.
1210 Liu, Q., X. Chen, M. K. Novak, S. Zhang, and W. Hu, 2021 Repressing Ago2 mRNA translation
1211 by Trim71 maintains pluripotency through inhibiting *let-7* microRNAs. Elife 10: e66288.
1212 Lorenz, S., 2018 Structural mechanisms of HECT-type ubiquitin ligases. Biol Chem 399: 127–
1213 145.
1214 Luong, X. G., and M. Conti, 2019 RNA binding protein networks and translational regulation in
1215 oocytes. In *Human Reproductive and Prenatal Genetics*, edited by P. C. K. Leung and J.
1216 Qiao. Academic Press, Cambridge.
1217 Maller Schulman, B. R., X. Liang, C. Stahlhut, C. DelConte, G. Stefani *et al.*, 2008 The *let-7*
1218 microRNA target gene, *Mlin41/Trim71* is required for mouse embryonic survival and
1219 neural tube closure. Cell Cycle 7: 3935–3942.
1220 Martínez-Noël, G., J. T. Galligan, M. E. Sowa, V. Arndt, T. M. Overton *et al.*, 2012
1221 Identification and proteomic analysis of distinct UBE3A/E6AP protein complexes. Mol
1222 Cell Biol 32: 3095–3106.

1223 Marín, I., 2018 Origin and evolution of fungal HECT ubiquitin ligases. Sci Rep 8: 6419.
1224 Matsuura, R., T. Ashikawa, Y. Nozaki, and D. Kitagawa, 2016 LIN-41 inactivation leads to
1225 delayed centrosome elimination and abnormal chromosome behavior during female
1226 meiosis in *Caenorhabditis elegans*. Mol Biol Cell 27: 799–811.
1227 McCarter, J., B. Bartlett, T. Dang, and T. Schedl, 1999 On the control of oocyte meiotic
1228 maturation and ovulation in *Caenorhabditis elegans*. Dev Biol 205: 111–128.
1229 McNally, K., A. Audhya, K. Oegema, and F. J. McNally, 2006 Katanin controls mitotic and
1230 meiotic spindle length. J Cell Biol 175: 881–891.
1231 Miller, M. A., V. Q. Nguyen, M.-H. Lee, M. Kosinski, T. Schedl *et al.*, 2001 A sperm
1232 cytoskeletal protein that signals oocyte meiotic maturation and ovulation. Science 291:
1233 2144–2147.
1234 Mitschka, S., T. Ulas, T. Goller, K. Schneider, A. Egert *et al.*, 2015 Co-existence of intact
1235 stemness and priming of neural differentiation programs in mES cells lacking Trim71.
1236 Sci Rep 5: 11126.
1237 Nance, J., and C. Frøkjær-Jensen, 2019 The *Caenorhabditis elegans* transgenic toolbox. Genetics
1238 212: 959–990.
1239 Newport, J., and M. Kirschner, 1982a A major developmental transition in early *Xenopus*
1240 embryos: I. Characterization and timing of cellular changes at the midblastula stage. Cell
1241 30: 675–686.
1242 Newport, J., and M. Kirschner, 1982b A major developmental transition in early *Xenopus*
1243 embryos: II. Control of the onset of transcription. Cell 30: 687–696.
1244 Nishi, Y., and R. Lin, 2005 DYRK2 and GSK-3 phosphorylate and promote the timely
1245 degradation of OMA-1, a key regulator of the oocyte-to-embryo transition in *C. elegans*.

1246 Dev Biol 288: 139–149.
1247 O'Farrell, F., S. S. Esfahani, Y. Engström, and P. Kylsten, 2008 Regulation of the *Drosophila*
1248 *lin-41* homologue *dappled* by *let-7* reveals conservation of a regulatory mechanism
1249 within the LIN-41 subclade. Dev Dyn 237: 196–208.
1250 Pritchard, D. K., and G. Schubiger, 1996 Activation of transcription in *Drosophila* embryos is a
1251 gradual process mediated by the nucleocytoplasmic ratio. Genes Dev 10: 1131–1142.
1252 Redemann, S., S. Schloissnig, S. Ernst, A. Pozniakowsky, S. Ayloo *et al.*, 2011 Codon
1253 adaptation-based control of protein expression in *C. elegans*. Nat Methods 8: 250–252.
1254 Reichard, E. L., G. G. Chirico, W. J. Dewey, N. D. Nassif, K. E. Bard *et al.*, 2016 Substrate
1255 ubiquitination controls the unfolding ability of the proteasome. J Biol Chem 291: 18547–
1256 18561.
1257 Reinhart, B. J., F. J. Slack, M. Basson, A. E. Pasquinelli, J. C. Bettinger *et al.*, 2000 The 21-
1258 nucleotide *let-7* RNA regulates developmental timing in *Caenorhabditis elegans*. Nature
1259 403: 901–906.
1260 Robertson, S., and R. Lin, 2013 The oocyte-to-embryo transition. Adv Exp Med Biol 757: 351–
1261 372.
1262 Robertson, S., and R. Lin, 2015 The maternal-to-zygotic transition in *C. elegans*. Curr Top Dev
1263 Biol 113: 1–42.
1264 Rose, K. L., V. P. Winfrey, L. H. Hoffman, D. H. Hall, T. Furuta *et al.*, 1997 The POU gene *ceh-*
1265 *18* promotes gonadal sheath cell differentiation and function required for meiotic
1266 maturation and ovulation in *Caenorhabditis elegans*. Dev Biol 192: 59–77.
1267 Rosu, S., and O. Cohen-Fix, 2017 Live-imaging analysis of germ cell proliferation in the *C.*
1268 *elegans* adult supports a stochastic model for stem cell proliferation. Dev Biol 423: 93–

1269 100.
1270 Rosu, S., and O. Cohen-Fix, 2020 Tracking germline stem cell dynamics *in vivo* in *C. elegans*
1271 using photoconversion. Methods Mol Biol 2150: 11–23.
1272 Rybak, A., H. Fuchs, K. Hadian, L. Smirnova, E. A. Wulczyn *et al.*, 2009 The *let-7* target gene
1273 mouse *lin-41* is a stem cell specific E3 ubiquitin ligase for the miRNA pathway protein
1274 Ago2. Nat Cell Biol 11: 1411–1420.
1275 Sarov, M., J. I. Murray, K. Schanze, A. Pozniakovski, W. Niu *et al.*, 2012 A genome-scale
1276 resource for *in vivo* tag-based protein function exploration in *C. elegans*. Cell 150: 855–
1277 866.
1278 Schneider, C. A., W. S. Rasband, and K. W. Eliceiri, 2012 NIH Image to ImageJ: 25 years of
1279 image analysis. Nat Methods 9: 671–675.
1280 Seydoux, G., and A. Fire, 1994 Soma-germline asymmetry in the distributions of embryonic
1281 RNAs in *Caenorhabditis elegans*. Development 120: 2823–2834.
1282 Sha, Q. Q., X. X. Dai, Y. Dang, F. Tang, J. Liu *et al.*, 2017 A MAPK cascade couples maternal
1283 mRNA translation and degradation to meiotic cell cycle progression in mouse oocytes.
1284 Development 144: 452–463.
1285 Shakes, D. C., P. L. Sadler, J. M. Schumacher, M. Abdolrasulnia, and A. Golden, 2003
1286 Developmental defects observed in hypomorphic anaphase-promoting complex mutants
1287 are linked to cell cycle abnormalities. Development 130: 1605–1620.
1288 Shirayama, M., M. C. Soto, T. Ishidate, S. Kim, K. Nakamura *et al.*, 2006 The conserved kinases
1289 CDK-1, GSK-3, KIN-19, and MBK-2 promote OMA-1 destruction to regulate the
1290 oocyte-to-embryo transition in *C. elegans*. Curr Biol 16: 47–55.
1291 Singh, S., and J. Sivaraman, 2020 Crystal structure of HECT domain of UBE3C E3 ligase and its

1292 ubiquitination activity. Biochem J 477: 905–923.
1293 Slack, F. J., M. Basson, Z. Liu, V. Ambros, H. R. Horvitz *et al.*, 2000 The *lin-41* RBCC gene
1294 acts in the *C. elegans* heterochronic pathway between the *let-7* regulatory RNA and the
1295 LIN-29 transcription factor. Mol Cell 5: 659–669.
1296 Spieth, J., G. Brooke, S. Kuersten, K. Lea, and T. Blumenthal, 1993 Operons in *C. elegans*:
1297 polycistronic mRNA precursors are processed by trans-splicing of SL2 to downstream
1298 coding regions. Cell 73: 521–532.
1299 Spike, C. A., D. Coetzee, C. Eichten, X. Wang, D. Hansen *et al.*, 2014a The TRIM-NHL protein
1300 LIN-41 and the OMA RNA-binding proteins antagonistically control the prophase-to-
1301 metaphase transition and growth of *Caenorhabditis elegans* oocytes. Genetics 198: 1535–
1302 1558.
1303 Spike, C. A., D. Coetzee, Y. Nishi, T. Guven-Ozkan, M. Oldenbroek *et al.*, 2014b Translational
1304 control of the oogenic program by components of OMA ribonucleoprotein particles in
1305 *Caenorhabditis elegans*. Genetics 198: 1513–1533.
1306 Spike, C. A., G. Huelgas-Morales, T. Tsukamoto, and D. Greenstein, 2018 Multiple mechanisms
1307 inactivate the LIN-41 RNA-binding protein to ensure a robust oocyte-to-embryo
1308 transition in *Caenorhabditis elegans*. Genetics 210: 1011–1037.
1309 Starostina, N. G., J. M. Lim, M. Schvarzstein, L. Lim, A. M. Spence *et al.*, 2007 A CUL-2
1310 ubiquitin ligase containing three FEM proteins degrades TRA-1 to regulate *C. elegans*
1311 sex determination. Dev Cell 13: 127–139.
1312 Stitzel, M. L., J. Pellettieri, and G. Seydoux, 2006 The *C. elegans* DYRK kinase MBK-2 marks
1313 oocyte proteins for degradation in response to meiotic maturation. Curr Biol 16: 56–62.
1314 Teixeira, F. K., and R. Lehmann, 2019 Translational control during developmental transitions.

1315 Cold Spring Harb Perspect Biol 11: a032987.
1316 The *C. elegans* Deletion Mutant Consortium, 2012 Large-scale screening for targeted knockouts
1317 in the *Caenorhabditis elegans* genome. G3 (Bethesda) 2: 1415–1425.
1318 Timmons, L., and A. Fire, 1998 Specific interference by ingested dsRNA. Nature 395: 854.
1319 Tocchini, C., J. J. Keusch, S. B. Miller, S. Finger, H. Gut *et al.*, 2014 The TRIM-NHL protein
1320 LIN-41 controls the onset of developmental plasticity in *Caenorhabditis elegans*. PLoS
1321 Genet 10: e1004533.
1322 Torres-Fernández, L. A., J. Emich, Y. Port, S. Mitschka, M. Wöste *et al.*, 2021a *TRIM71*
1323 deficiency causes germ cell loss during mouse embryogenesis and is associated with
1324 human male infertility. Front Cell Dev Biol 9: 658966.
1325 Torres-Fernández, L. A., S. Mitschka, T. Ulas, S. Weise, K. Dahm *et al.*, 2021b The stem cell-
1326 specific protein TRIM71 inhibits maturation and activity of the pro-differentiation
1327 miRNA *let-7* via two independent molecular mechanisms. RNA 27: 805–828.
1328 Tsien, R. Y., 1998 The green fluorescent protein. Annu Rev Biochem 67: 509–544.
1329 Tsukamoto, T., M. D. Gearhart, C. A. Spike, G. Huelgas-Morales, M. Mews *et al.*, 2017 LIN-41
1330 and OMA ribonucleoprotein complexes mediate a translational repression-to-activation
1331 switch controlling oocyte meiotic maturation and the oocyte-to-embryo transition in
1332 *Caenorhabditis elegans*. Genetics 206: 2007–2039.
1333 van der Voet, M., M. A. Lorson, D. G. Srinivasan, K. L. Bennett, and S. van den Heuvel, 2009
1334 *C. elegans* mitotic cyclins have distinct as well as overlapping functions in chromosome
1335 segregation. Cell Cycle 8: 4091–4102.
1336 Wang, R., Z. Kaul, C. Ambardekar, T. G. Yamamoto, K. Kavdia *et al.*, 2013 HECT-E3 ligase
1337 ETC-1 regulates securin and cyclin B1 cytoplasmic abundance to promote timely

1338 anaphase during meiosis in *C. elegans*. Development 140: 2149–2159.
1339 Ward, S., Y. Argon, and G. A. Nelson, 1981 Sperm morphogenesis in wild-type and fertilization-
1340 defective mutants of *Caenorhabditis elegans*. J Cell Biol 91: 26–44.
1341 Welcker, M., and B. E. Clurman, 2008 FBW7 ubiquitin ligase: a tumour suppressor at the
1342 crossroads of cell division, growth and differentiation. Nat Rev Cancer 8: 83–93.
1343 Welcker, M., A. Orian, J. E. Grim, J. A. Grim, R. N. Eisenman *et al.*, 2004 A nucleolar isoform
1344 of the Fbw7 ubiquitin ligase regulates c-Myc and cell size. Curr Biol 14: 1852–1857.
1345 Worringer, K. A., T. A. Rand, Y. Hayashi, S. Sami, K. Takahashi *et al.*, 2014 The *let-7*/LIN-41
1346 pathway regulates reprogramming to human induced pluripotent stem cells by controlling
1347 expression of prodifferentiation genes. Cell Stem Cell 14: 40–52.
1348 Yoon, S., I. Kawasaki, and Y. H. Shim, 2017 The B-type cyclin CYB-1 maintains the proper
1349 position and number of centrosomes during spermatogenesis in. J Cell Sci 130: 2722–
1350 2735.
1351 You, J., and C. M. Pickart, 2001 A HECT domain E3 enzyme assembles novel polyubiquitin
1352 chains. J Biol Chem 276: 19871–19878.
1353 You, J., M. Wang, T. Aoki, T. A. Tamura, and C. M. Pickart, 2003 Proteolytic targeting of
1354 transcriptional regulator TIP120B by a HECT domain E3 ligase. J Biol Chem 278:
1355 23369–23375.
1356 Zavortink, M., L. N. Rutt, S. Dzitoyeva, J. C. Henriksen, C. Barrington *et al.*, 2020 The E2
1357 Marie Kondo and the CTLH E3 ligase clear deposited RNA binding proteins during the
1358 maternal-to-zygotic transition. Elife 9: e53889.
1359 Zevian, S. C., and J. L. Yanowitz, 2014 Methodological considerations for heat shock of the
1360 nematode *Caenorhabditis elegans*. Methods 68: 450–457.

1361 **FIGURE LEGENDS**

1362 Figure 1. SEL-10 is expressed in oocytes and embryos and promotes the degradation of
1363 mSCARLET::LIN-41 during the OET. mSCARLET::LIN-41 (A, B, D, F, I, and L), GFP::SEL-
1364 10 (C and H) and SEL-10::GFP (E and K) fluorescence in *C. elegans* germlines (solid outlines)
1365 and early embryos (dashed outlines). mSCARLET::LIN-41 is rapidly degraded after oogenesis in
1366 the wild type (A) and *sel-10(tn1875[gfp::3xflag::sel-10])* (D) hermaphrodites but persists in
1367 early embryos in the *sel-10(ok1632)* deletion (B) and *sel-10(tn1817[sel-10::gfp::3xflag])* (F)
1368 hermaphrodites. Embryos with an increased amount of mSCARLET::LIN-41 relative to *sel-*
1369 *10(+)* embryos are outlined in magenta (B and F). Magnified image insets of the selected regions
1370 (C–F) are shown for GFP::SEL-10 (G–I) and for SEL-10::GFP (J–L), respectively. Differential
1371 interference contrast microscopic images are shown (G and J) to highlight germ cell nucleoli
1372 (yellow arrows). The circled nucleoli (G–L) lie in the middle focal plane of a germ cell nucleus,
1373 illustrating that functional GFP::SEL-10 is enriched in the nucleoplasm but largely excluded
1374 from nucleoli (G–I). Non-functional SEL-10::GFP is also excluded from nucleoli but is not
1375 enriched in the nucleoplasm relative to the cytoplasm at this stage of oocyte development (J–L).
1376 mSCARLET::LIN-41 is exclusively cytoplasmic and excluded from nuclei (I and L). Landmark
1377 structures such as the distal mitotic region of the germline (arrow in A), the proximal-most
1378 oocytes (arrowheads in A) and the spermatheca (sp), are indicated for reference. Scale bars,
1379 100 μm (A–F) and 10 μm (G–L), respectively.

1380

1381 Figure 2. SEL-10 degrades oocyte-expressed DENDRA::LIN-41. Red and green channel
1382 fluorescence (A–C and F–H) in DENDRA::LIN-41-expressing *sel-10(ok1632)* (A–E) and *sel-*

1383 *10(+)* (F–J) hermaphrodites. The positions of oocytes (solid outlines), embryos (dashed outlines)
1384 and spermathecae (sp) are indicated for reference. Images were collected either before
1385 photoactivation (A and F), immediately after photoactivation of the −1 oocyte (arrowheads, B
1386 and G) or after a 100-min recovery period (C–E and H–J). Embryos with above-background
1387 levels of red channel fluorescence are outlined in magenta; the embryo that most likely
1388 developed from the photoactivated −1 oocyte is indicated with an arrowhead (C and H).
1389 Magnified red channel fluorescence (D and I) and DIC images (E and J) of this embryo are
1390 shown. Scale bars, 50 μm (A–C and F–H) and 20 μm (D, E, I, and J).

1391

1392 Figure 3. PUF-11::GFP and PUF-3::GFP are degraded during the OET. (A–F) PUF-11::GFP (A),
1393 PUF-3::GFP (D and G) and mSCARLET::LIN-41 (B and E) fluorescence in *C. elegans*
1394 germlines (solid outlines) and early embryos (dashed outlines). The arrow in (A and D) indicates
1395 the distal mitotic region of each germline. Merged images of (A and B) and (D and E) are shown
1396 in (C) and (F), respectively. (G–J) Images of *itIs37[pie-1p::mcherry::histoneH2B::pie-1 3'UTR,*
1397 *unc-119(+)] puf-3(tn1820[puf-3::gfp::3xflag])* oocytes and embryos reveal that PUF-3::GFP (G)
1398 is strongly reduced in a meiosis I stage embryo (MI) relative to the −1 oocyte. Chromosomes are
1399 marked with mCHERRY:HISTONE (H), and the oocyte-derived chromosomes in this MI
1400 embryo appear to be aligning on the metaphase plate. PUF-3::GFP is at background levels in the
1401 adjacent post-meiotic 1-cell embryo (pn); this embryo has two polar bodies and maternal and
1402 paternal pronuclei at opposite ends of the embryo. Merged and DIC images of the same oocytes
1403 and embryos are shown in (I) and (J), respectively. The fluorescent images in this series (G–I)
1404 are 3D projections of a Z-stack. The DIC image (J) shows a single focal plane. Embryos with

1405 slightly higher levels of GFP and mSCARLET relative to older embryos are outlined in green
1406 and magenta, respectively (D, E, and G–J). Scale bars, 100 μm (A–F) and 50 μm (G–J). (K)
1407 PUF-3::GFP levels decrease after meiotic resumption. Mean GFP fluorescence was measured in
1408 images of *itIs37[pie-1p::mcherry::histoneH2B::pie-1 3'UTR] puf-3(tn1820)* oocytes and
1409 embryos and background-corrected. Fluorescence intensity is expressed relative to the amount of
1410 GFP fluorescence in the oldest oocyte with an intact nucleus; this is the –2 oocyte if the –1
1411 oocyte has initiated nuclear envelope breakdown (NEBD) or is starting to move into the
1412 spermatheca (early ovulation stage). Embryonic meiotic stage (e.g., metaphase I, telophase I and
1413 metaphase II) was classified based on the arrangement and organization of maternal
1414 chromosomes.

1415

1416 Figure 4. The elimination of PUF-3::GFP and PUF-11::GFP requires active CDK-1 but does not
1417 require SEL-10. PUF-3::GFP (A–D) and PUF-11::GFP (E–H) fluorescence in *C. elegans*
1418 germlines (solid outlines) and early embryos (dashed outlines) in *cdk-1(RNAi)* (A and E), *wee-*
1419 *1.3(RNAi)* (B and F), *lon-3(e2175)* (C and G) and *lon-3(e2175) sel-10(ar41)* (D and H)
1420 hermaphrodites. For each GFP fusion protein, the images of the *lon-3(e2175)* and *lon-3(e2175)*
1421 *sel-10(ar41)* animals were collected using the same settings (e.g., C and D). Embryos that appear
1422 GFP-positive are outlined in green. The slight reduction of PUF-3/11::GFP levels in more
1423 proximally located (i.e., older) arrested embryos in the uterus (A and E) might reflect CDK-1-
1424 independent turnover or it could result from residual CDK-1 activity following the RNAi
1425 treatment. The position of the spermatheca (sp) is indicated for reference. Arrowheads indicate
1426 the most proximal oocyte in each *wee-1.3(RNAi)* gonad that is strongly GFP-positive. (I) This
1427 graph illustrates the relative position of the most proximal mSCARLET or GFP-positive oocyte

1428 in 12 different *lin-41(tn1892[mScarlet::3xflag::lin-41]); puf-11(tn1824[puf-11::gfp::3xflag]);*
1429 *wee-1.3(RNAi)* animals. *wee-1.3(RNAi)* animals with well-formed and organized oocytes were
1430 scored. Oocyte position was measured relative to other oocytes and the spermatheca (position 0).
1431 Each animal is represented by a different symbol (e.g., filled diamond or open circle). The
1432 selection of a filled or open symbol is arbitrary and made to depict the 12 animals scored with six
1433 symbol shapes. The color of the symbol represents the fusion protein that was scored:
1434 mSCARLET::LIN-41 in magenta and PUF-3::GFP in green. The vertical bar indicates the
1435 median. Scale bars, 50 μm (A–H).

1436

1437 Figure 5. *etc-1(gk5182)* perturbs the degradation of GFP-fusion proteins during the OET. PUF-
1438 3::GFP (A and B), PUF-11::GFP (C and D), mSCARLET::LIN-41 (E and F), CYB-1::GFP (G
1439 and H), IFY-1::GFP (I and J) and GFP_F::LIN-41 (K and L) fluorescence in young *etc-1(+)* (A, C,
1440 E, G, I, and K) and *etc-1(gk5182)* (B, D, F, H, J, and L) embryos. In each image, the position of
1441 the spermatheca (sp) is indicated for reference. Young embryos in the uterus are indicated with
1442 dashed outlines that highlight individual embryos (A–H, K, and L) or a bracket that indicates a
1443 region containing multiple post-meiotic embryos (I and J). GFP-positive embryos are indicated
1444 in green (A–D and G–L) while mSCARLET-positive embryos are indicated in magenta (E and
1445 F). For each fusion protein, these embryos contain detectably more fluorescence than the *etc-*
1446 *1(+)* embryos indicated in white. CYB-1::GFP re-accumulates to relatively high levels in older
1447 *etc-1(+)* embryos (G, arrowhead; this embryo is no longer in the uterus) and therefore has a
1448 distinctly different expression pattern than the other OET-degraded fusion proteins. Scale bars,
1449 50 μm.

1450 Figure 6. ETC-1 is expressed in the *C. elegans* germline. (A) *etc-1* alleles and the exon-intron
1451 structure of *etc-1*, the downstream gene in operon CEOP2380. Exons are shown as open boxes;
1452 the region of exon 1 colored in pink would encode 20 additional amino acids if translation is
1453 initiated at ATG #1, the start codon immediately adjacent to the annotated SL1/SL2 trans-splice
1454 site (orange), instead of ATG #2. Other colors indicate the 3' UTR of the upstream gene eIF-2B
1455 (gray) and the regions that encode the conserved IQ (purple) and HECT (yellow) domains of
1456 ETC-1. (B) The N-terminus of ETC-1 aligned with the N-terminus of the human ortholog
1457 UBE3C; the amino acids predicted to be added to ETC-1 are in pink. This is the N-terminal
1458 portion of a full-length protein alignment generated by EMBOSS Needle with default alignment
1459 parameters. ETC-1 and UBE3C were 26% identical or 46% similar overall with 16% of the
1460 alignment gapped. (C and D) GFP::ETC-1 fluorescence in *C. elegans* germlines (solid outlines)
1461 and early embryos (dashed outlines). GFP is N-terminal to either the first (C, *etc-*
1462 *1(tn1919[gfp::3xflag::etc-1 #1])*) or second (D, *etc-1(tn1920[gfp::3xflag::etc-1#2])*) methionine
1463 of ETC-1. Scale bars, 100 μm. (E) A western blot of GFP::ETC-1 (~150 kDa, see main text) and
1464 PUF-3::GFP-expressing strains with an anti-FLAG antibody that recognizes both fusion proteins.
1465 GFP::FLAG fragments derived from PUF-3::GFP strongly accumulate in *etc-1(gk5182)* and *etc-*
1466 *1(tn1920[gfp::3xflag::etc-1#2])* hermaphrodites.

1467

1468 Figure 7. GFP-tagged fusion proteins are partially proteolyzed in *etc-1(gk5182)* animals. (A–E)
1469 Western blots with a FLAG-specific primary antibody. Three FLAG tags are located at the
1470 extreme C-terminus of PUF-3::GFP, PUF-11::GFP, CYB-1::GFP and IFY-1::GFP and in-
1471 between LIN-41 and each fluorescent protein (mSCARLET, DENDRA, or GFP). The predicted
1472 molecular mass of each full-length fusion protein (vertical line) is ~89 kDa for each PUF::GFP

1473 fusion protein (A and B), 73 kDa for CYB-1::GFP (A and B), 61 kDa for IFY-1::GFP (C), and
1474 154–156 kDa for each LIN-41 fusion protein (D and E), and. The same set of molecular weight
1475 markers (horizontal lines) were used in (A) and (B). A partially proteolyzed GFP::FLAG-
1476 containing fragment >32 kDa (arrow) accumulates in the *etc-1(gk5182)* animals that express a
1477 GFP fusion protein (A, B, C, and E). The protein lysates were made from adult hermaphrodites
1478 (A, C, D, and E), adult females (B) or adult males (B), as indicated.

1479

1480 **LEGENDS TO SUPPLEMENTAL FIGURES**

1481 Figure S1. Alleles used in this study. (A) The exon-intron structures and allele names of the *sel-*
1482 *10* alleles used in this study. Exons are shown as open boxes. Colored regions of the *sel-10* exons
1483 encode the conserved F box (orange) and 7 WD repeat (gray) domains found in SEL-10. The
1484 GFP and FLAG-encoding regions added to the GFP-tagged alleles are colored in green and cyan,
1485 respectively. (B) The exon-intron structures and allele names of the *lin-41* alleles used in this
1486 study. Colored regions of the *lin-41* exons encode the conserved RING (yellow), B-box (orange),
1487 BBC (blue), Ig/filamin (purple) and NHL repeats (red) domains found in LIN-41. Fusion protein
1488 tags include GFP (green), S tag (gray), mSCARLET-I (brick red), FLAG tag (cyan) and
1489 DENDRA (green to red color gradient). (C) The exon-intron structures and allele names of *puf-*
1490 *3::gfp::3xflag*, *puf-11::gfp::3xflag*, *cyb-1::gfp::3xflag* and *rnp-8::gfp::3xflag*. The Pumilio-like
1491 repeats of PUF-3 and PUF-11 are in yellow. The Cyclin-N and Cyclin-C motifs of CYB-1 are in
1492 blue and orange, respectively. The RNA recognition motif (RRM) present in RNP-8 is in purple.
1493 As in prior panels, the GFP and FLAG protein tags are in green and cyan, respectively.

1494

1495 Figure S2. GLD-1 is degraded normally in *sel-10(tn1875[gfp::3xflag::sel-10])* animals.
1496 Dissected wild-type (A and C), *sel-10(tn1875[gfp::3xflag::sel-10])* (B) and *sel-10(tn1816[sel-*
1497 *10::gfp::3xflag])* (D) gonads (solid outlines) that have been fixed and stained with an anti-GLD-
1498 1 antibody. Each gonad is oriented so that the distal mitotic region is on the left and the proximal
1499 oocyte-containing region is on the right. Two different wild-type gonads are shown because
1500 slightly different staining and imaging conditions were used for each experiment; wild-type

1501 image A pairs with *sel-10(tn1875[gfp::3xflag::sel-10])* (A-B) and wild-type image C pairs with
1502 *sel-10(tn1816[sel-10::gfp::3xflag])* (C and D). Scale bars, 50 μm.

1503

1504 Figure S3. The elimination of PUF-3/11::GFP proteins during the OET. (A–C) GFP expression
1505 in *puf-11(tn1824[puf-11::gfp::3xflag])* (A), *puf-3(tn1820[puf-3::gfp::3xflag])* (B) and *puf-*
1506 *11(tn1824); puf-3(tn1820)* (C) animals. GFP-positive embryos are outlined in green. The
1507 position of the spermatheca (sp) is indicated (A). All images were collected using the same
1508 settings. (D and E) Quantification of GFP fluorescence levels in arbitrary units across the distal
1509 and proximal gonad for the three genotypes analyzed: *puf-11(tn1824[puf-11::gfp::3xflag])*
1510 (magenta); *puf-3(tn1820[puf-3::gfp::3xflag])* (blue); and *puf-11(tn1824); puf-3(tn1820)* (black).
1511 These quantitative data indicate that PUF-11::GFP accounts for the expression in the distal
1512 gonad, whereas both PUF-11::GFP and PUF-3::GFP are expressed at similar levels in oocytes.
1513 Scale bars, 100 μm.

1514

1515 Figure S4. Degradation of PUF-3::GFP and PUF-11::GFP during the OET do not require
1516 function of an Skp, Cullin, F-box (SCF)-containing E3 ubiquitin ligase or the anaphase-
1517 promoting complex. PUF-3::GFP (A–D) or PUF-11::GFP (G–J) were analyzed after empty
1518 vector control RNAi (A and G), *cul-1(RNAi)* (B and H), *skr-1/2(RNAi)* (C and I), or *mat-1(RNAi)*
1519 (D and J). Additionally, PUF-3::GFP was analyzed at 25°C in *emb-30(tn377*ts*)*; *puf-*
1520 *3(tn1820[puf-3::gfp::3xflag])* (F), with *puf-3(tn1820[puf-3::gfp::3xflag])* as the control (E). The
1521 position of the spermatheca (sp) is indicated. Scale bars, 100 μm.

1522 Figure S5. GFP-expressing alleles of *etc-1*. (A) The exon-intron structures and allele names of
1523 the *gfp::3xflag::etc-1* alleles used in this study. Colors and labels are as described for Figure 6,
1524 with the addition of exons (open boxes) that encode the GFP (green) and FLAG (cyan) tags. (C
1525 and D) GFP fluorescence in *etc-1(tn1919[gfp::3xflag::etc-1#1])* (C) and *etc-*
1526 *1(tn1920[gfp::3xflag::etc-1#2])* (D) hermaphrodites. These are larger versions of the images
1527 shown in Figure 7 that include the region of somatic GFP expression in the head (arrow) that is
1528 significantly brighter in *etc-1(tn1920)* hermaphrodites. GFP expression in the nucleus of an
1529 intestinal cell is also evident in the focal plane of the *etc-1(tn1919)* image (arrowhead).
1530 Additional somatic cells also express GFP::ETC-1, but most of these cells were not identified.
1531 Scale bars, 100 μm.

1532

1533 Figure S6. Genetic interaction between *etc-1(tn2077)* and *mat-1(ax161*ts*)*. (A–D and A'–D')
1534 DIC images of day-1 (25°C) and day-2 (15°C) adult hermaphrodites of the indicated genotypes.
1535 Panels (A'–D') show increased magnification (1.5X) of the worms shown in panels (A–D) to
1536 focus on embryos within the uterus. Arrowheads indicate multicellular embryos. The position of
1537 the spermatheca (sp) is indicated. Scale bars, 50 μm.

1538

1539 Figure S7. Additional western blots related to Figure 7. (A) A western blot that repeats the
1540 experiment shown in Figure 7A and includes wild type and *etc-1(gk5182)* lanes with no
1541 GFP::FLAG fusion protein. (B) PUF-3::GFP, PUF-11::GFP, and CYB-1:: GFP fusion proteins
1542 (lines) and *etc-1(gk5182)*-specific GFP::FLAG fragments (arrows) are detected by an affinity
1543 purified antibody that recognizes GFP. (C and D) Western blots with the anti-FLAG antibody on

1544 GFP fusion protein-expressing hermaphrodites (C), mated *fog-2(oz40)* females (C), unmated *fog-*
1545 *2(oz40)* females (D) and *fog-2(oz40)* males (D) with the indicated *etc-1* genotypes. For unknown
1546 reasons, the RNP-8::GFP fusion protein detected in (C) appears to be slightly larger than
1547 predicted. The predicted size of the large RNP-8a isoform (see http://www.wormbase.org,
1548 release WS278) fused to the GFP::3xFLAG tag is 97 kDa. The blots shown in (D) and Figure 7B
1549 are the same; Figure 7B shows a shorter exposure of the portion of the blot with the female
1550 lysates and a longer exposure of the blot with the male CYB-1::GFP lysates. (E) A longer
1551 exposure of the western blot shown in Figure 7D that also includes otherwise wild-type, *etc-*
1552 *1(gk5182)* and *sel-10(lf)* animals that express DENDRA::LIN-41. (F) A longer exposure of the
1553 western blot shown in Figure 7E. *etc-1(+)* animals that express GFP_F::LIN-41 appear to
1554 accumulate a lesser amount of the GFP::FLAG fragment seen in *etc-1(gk5182)* animals. *etc-*
1555 *1(gk5182)*-specific fragments containing GFP::FLAG are indicated by arrows.

1556

1557 Figure S8. CYB-1::GFP expression in males. (A–F) CYB-1::GFP expression in *etc-1(+)* males
1558 (A) and *etc-1(gk5182)* males (C and F). CYB-1::GFP disappears abruptly in *cyb-1(tn1806[cyb-*
1559 *1::gfp::3xflag]); fog-2(oz40)* males (A and B) near the end of spermatogenesis (red boxes). At
1560 the same stage of spermatogenesis, *etc-1(gk5182)*; *cyb-1(tn1806[cyb-1::gfp::3xflag]); fog-*
1561 *2(oz40)* males (C–F) have higher levels of GFP fluorescence (C) and GFP-positive residual
1562 bodies (e.g., arrows in E and F). Scale bars, 50 μm (A–D) and 10 μm (E and F).

1563

1564 Figure S9. Additional images of GFP-tagged fusion proteins. (A and B) GFP is expressed at
1565 similar levels in the germlines (solid outlines) and early embryos (dashed outlines) of *rnp-*

1566 *8(tn1860[rpn-8::gfp::3xflag])* (A) and *etc-1(gk5182); rnp-8(tn1860[rpn-8::gfp::3xflag])* (B)
1567 hermaphrodites. (C and D) GFP fluorescence from *lin-41(tn1541[gfp::s::lin-41])* is distinctly
1568 brighter in the early embryos (dashed outlines) of *etc-1(gk5182)* hermaphrodites (D) relative to
1569 *etc-1(+)* hermaphrodites (C). (E–H) The GFP_S-tagged allele *lin-41(tn1541[gfp::s::lin-41])* (E)
1570 and GFP_F-tagged allele *lin-41(tn2054[gfp::3xflag::lin-41])* (G) have different levels of GFP
1571 expression. The average GFP fluorescence intensity in the cytoplasm of the −1 and −2 oocytes of
1572 *lin-41(tn2054)* and *lin-41(tn1541)* Day 1 adult hermaphrodites was measured (n=7 images for
1573 each allele, collected as shown). At each oocyte position (−1 or −2), the average background-
1574 corrected level of fluorescence was 2.4-fold higher in *lin-41(tn2054)* oocytes relative to *lin-*
1575 *41(tn1541)* oocytes ($P < 1 \times 10^{-6}$). Many *lin-41(tn2054[gfp::3xflag::lin-41])* Day 1 adult
1576 hermaphrodites also accumulate older embryos in their uterus (H) and appear to be sluggish.
1577 These phenotypes are shared by the independently-generated *lin-41(tn2055[gfp::3xflag::lin-41]*
1578 allele. At 20 °C, 43% and 62% of DG5263 *lin-41(tn2055)* Day 1 and Day 2 adults (n=29),
1579 respectively, had an egg laying (Egl) defect associated with premature mortality (dead on Day 2,
1580 3, or 4 of adulthood) and a reduced number of progeny (52 ± 21 larvae, n=18 Egl adults; 256 ±
1581 61 larvae, n=11 non-Egl adults). These somatic defects are not typically seen in *lin-*
1582 *41(tn1541[gfp::s::lin-41])* animals at the same stage of adulthood (F), and the average brood size
1583 of *lin-41(tn1541)* animals is greater than 300 (Spike *et al.* 2014a, 2018). (I–N) GFP fluorescence
1584 (I, K, and M) and DIC (J, L, and N) images of 2-cell *lin-41(tn2055[gfp::3xflag::lin-41])*
1585 embryos produced by otherwise wild-type (I and J), *etc-1(gk5182)* (K and L) and *sel-10(ok1632)*
1586 (M and N) parents. GFP is diffusely cytoplasmic in each embryo and is distinctly brighter in the
1587 *etc-1(gk5182)* and *sel-10(ok1632)* embryos relative to the wild-type embryo. Nuclear GFP
1588 (arrowheads) is evident in wild-type (I) and *etc-1(gk5182)* (K) embryos. In contrast, some GFP

1589 in the posterior blastomere of the *sel-10(ok1632)* embryo (M) appears to associate with P
1590 granules (arrow). The position of the spermatheca (sp) is indicated. Scale bars, 50 μm (A–H) and
1591 10 μm (I–N).

1592

1593 Table S1. *C. elegans* strains used in this study.

1594

1595 File S1. Information on the repair templates, single guide RNA plasmids, PCR primers, and the
1596 RNAi clones used in this study.

1597

1598 File S2. The nucleotide and amino acid sequences of fluorophore tags, tagged alleles, and
1599 deletion alleles used in this study.

1600

Figure 1

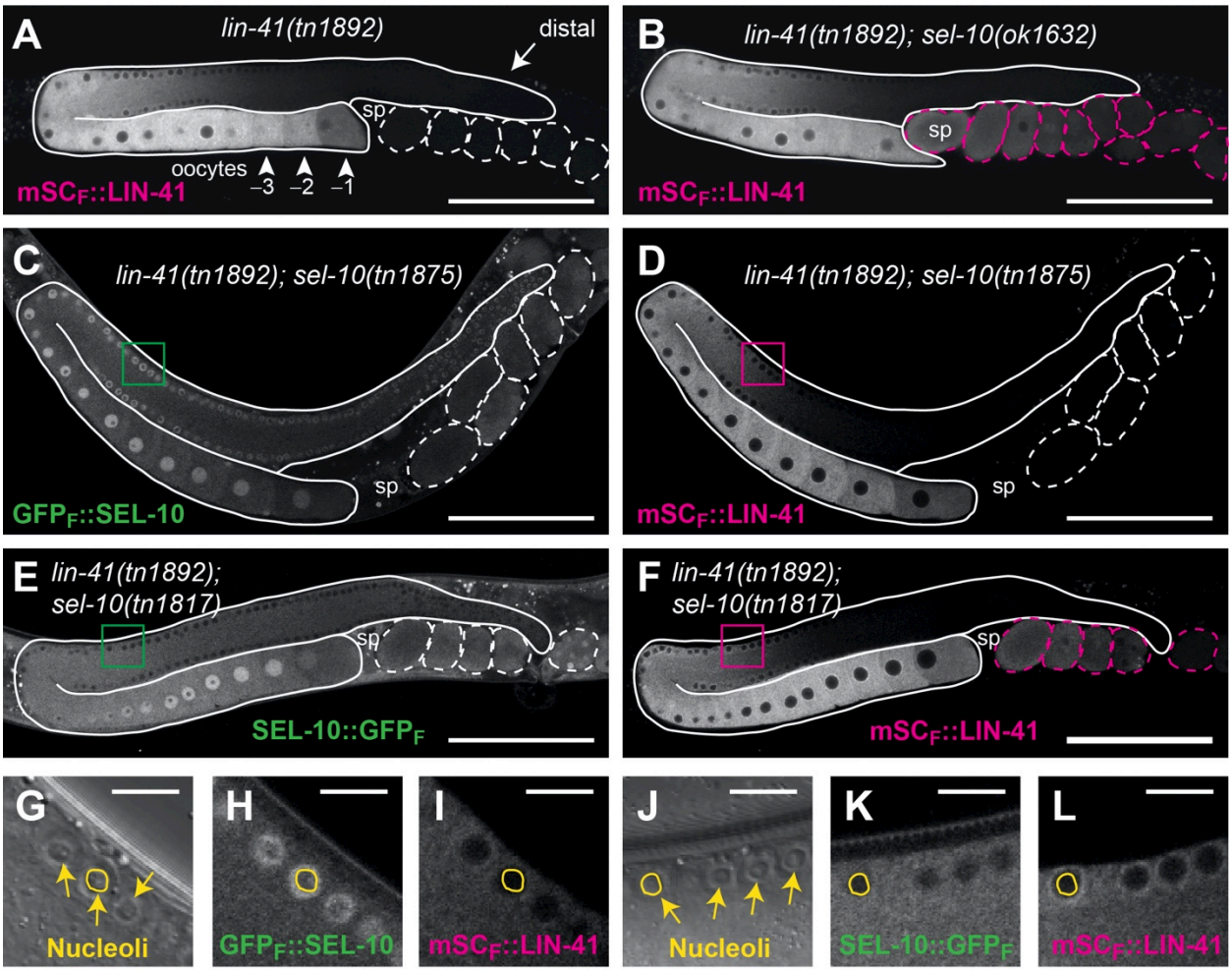
A
lin-41(tn1892)
distal
sp
oocytes
–3 –2 –1
mSCF::LIN-41
B
lin-41(tn1892); sel-10(ok1632)
sp
mSCF::LIN-41
C
lin-41(tn1892); sel-10(tn1875)
sp
GFPF::SEL-10
D
lin-41(tn1892); sel-10(tn1875)
sp
mSCF::LIN-41
E
lin-41(tn1892);
sel-10(tn1817)
sp
SEL-10::GFPF
F
lin-41(tn1892);
sel-10(tn1817)
sp
mSCF::LIN-41
G
Nucleoli
H
GFPF::SEL-10
I
mSCF::LIN-41
J
Nucleoli
K
SEL-10::GFPF
L
mSCF::LIN-41

Figure 2

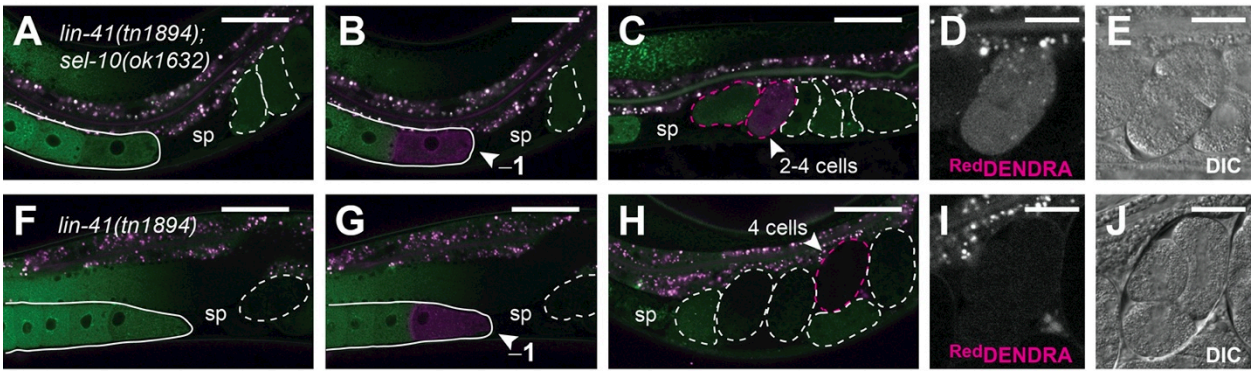
A
lin-41(tn1894);
sel-10(ok1632)
sp
B
sp
–1
C
sp
2-4 cells
D
RedDENDRA
E
DIC
F
lin-41(tn1894)
sp
G
sp
–1
H
4 cells
sp
I
RedDENDRA
J
DIC

Figure 3

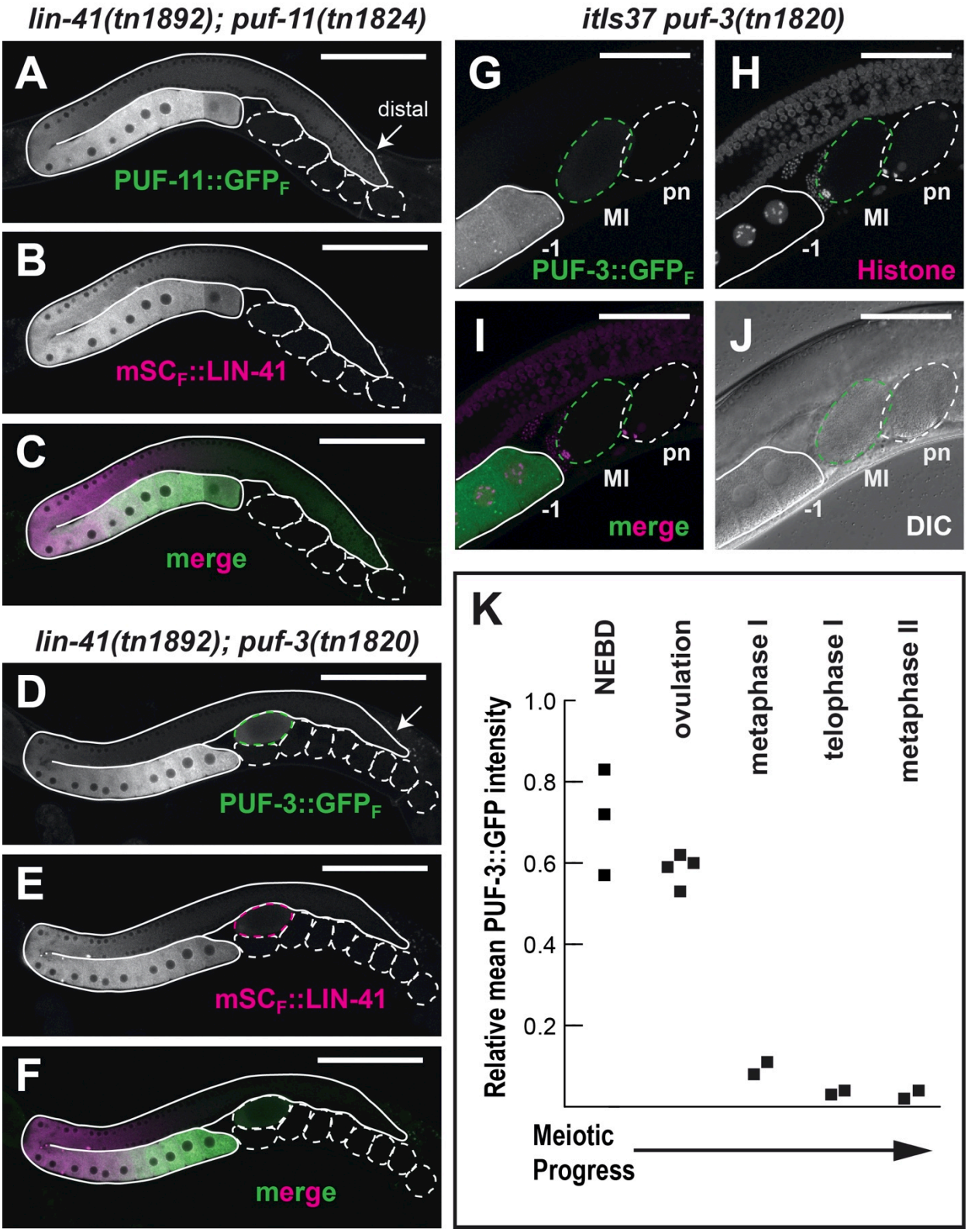

1605

Figure 4

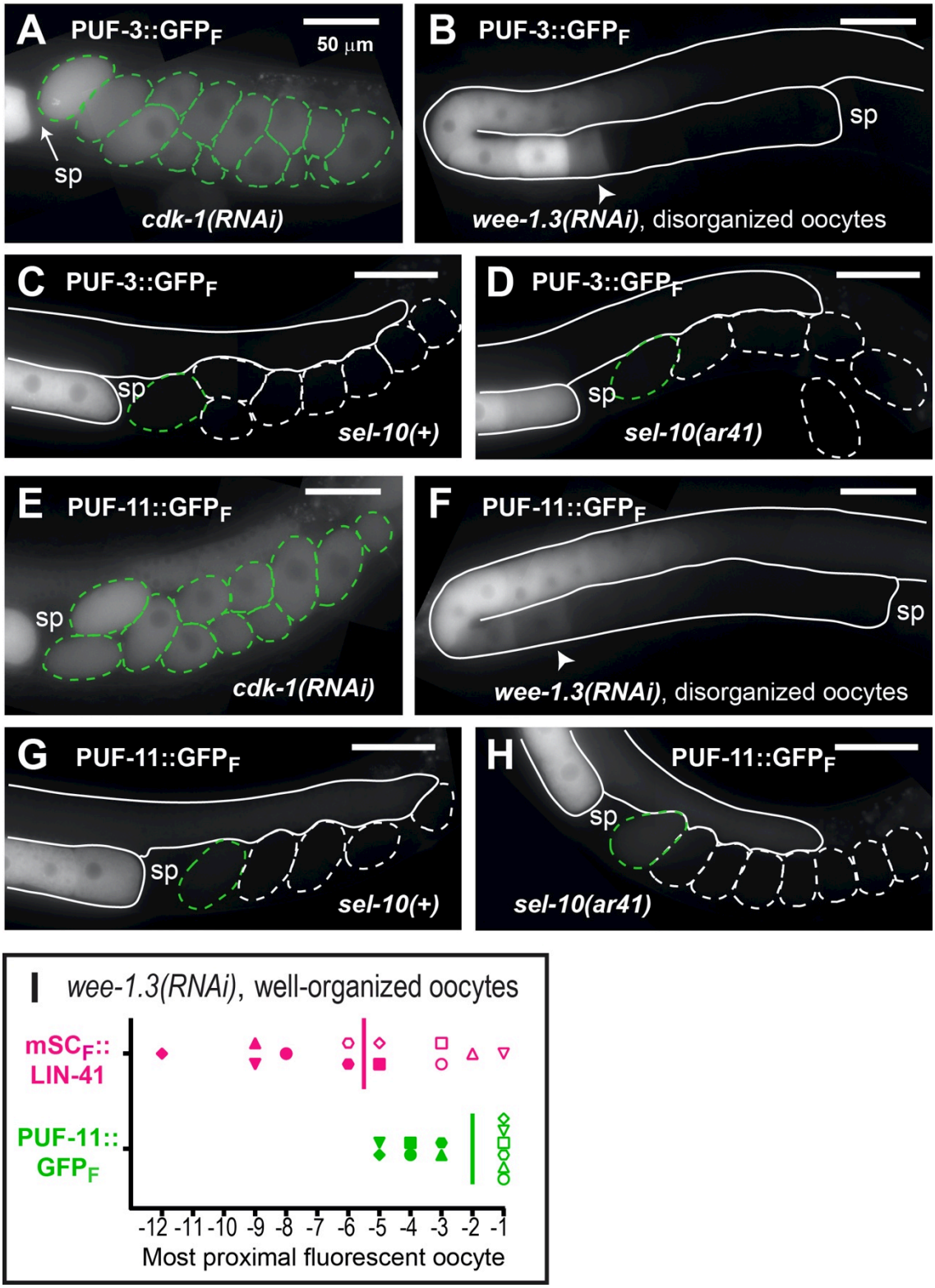

1606

Figure 5

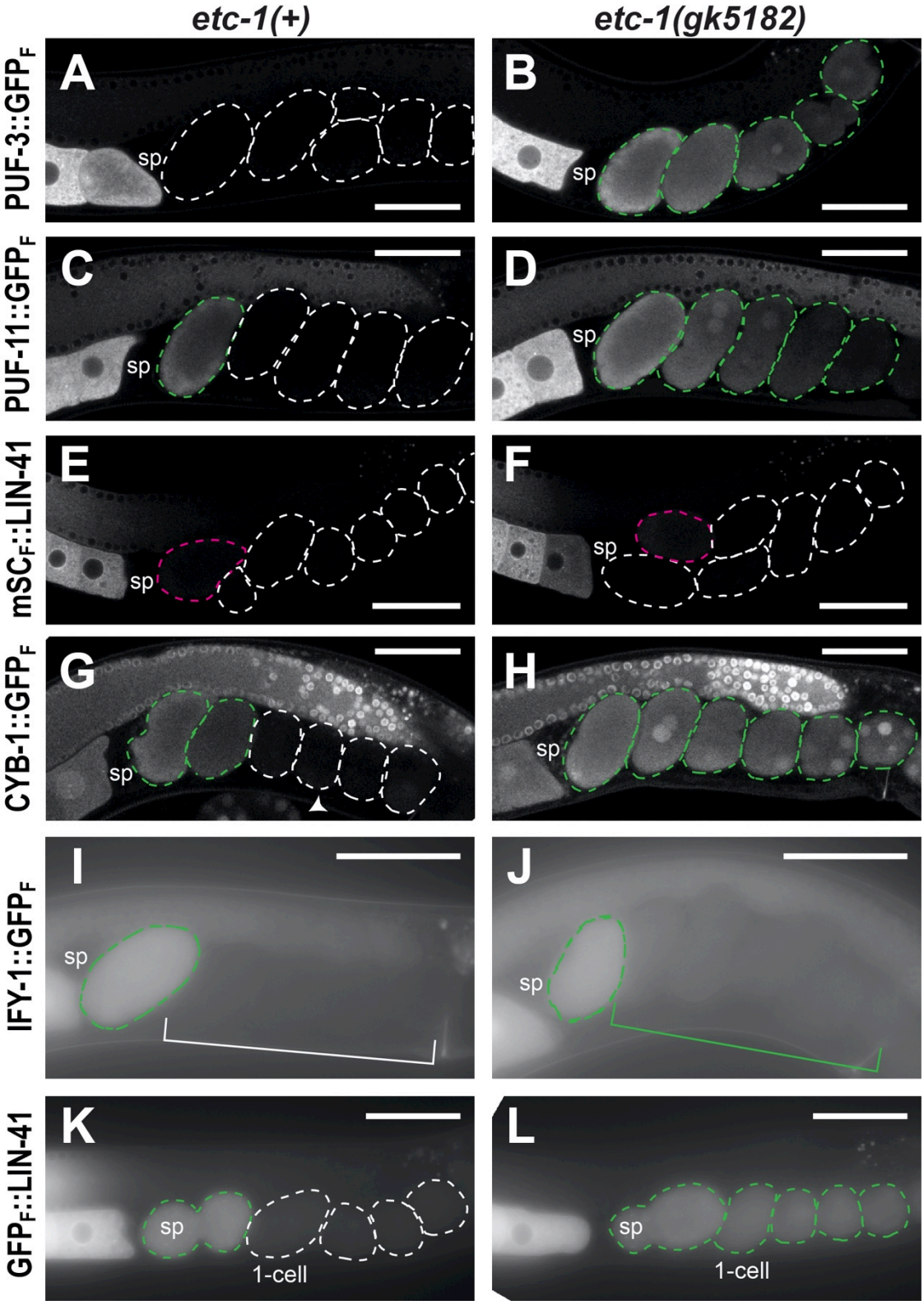

1607

Figure 6

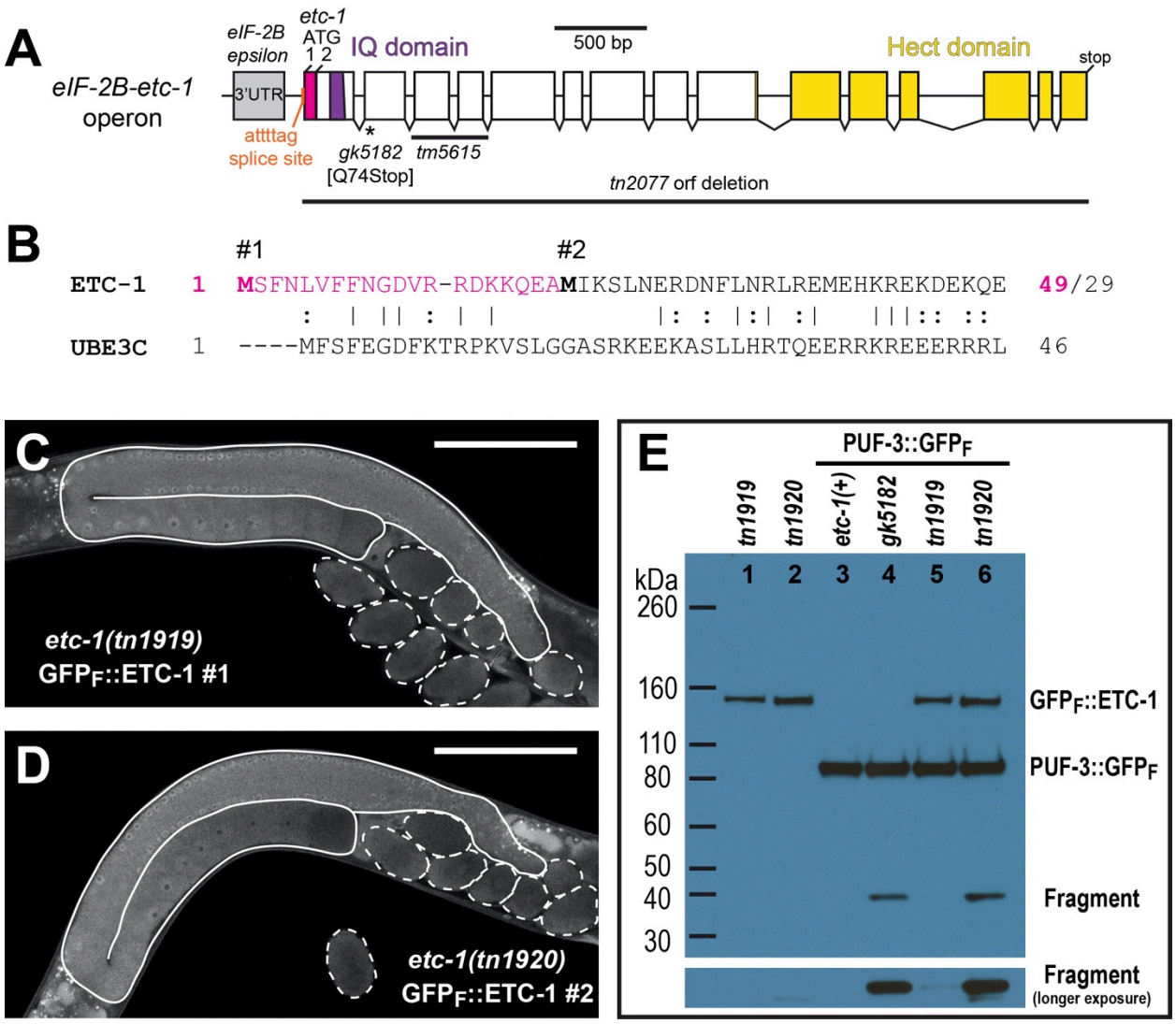

1608

1609

Figure 7

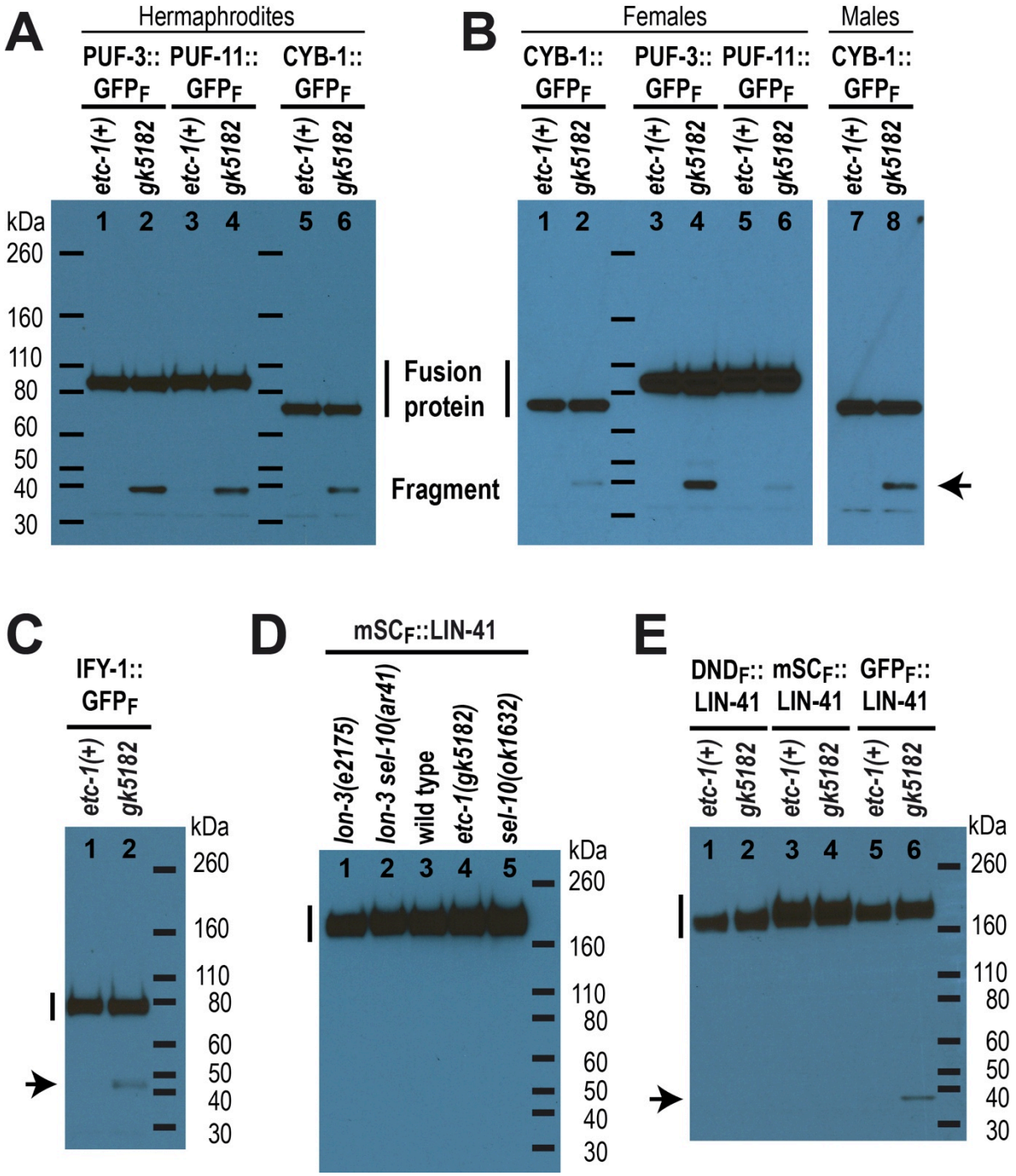
A
Hermaphrodites
PUF-3:: GFPF
PUF-11:: GFPF
CYB-1:: GFPF
etc-1(+)
gk5182
kDa
260
160
110
80
60
50
40
30
Fusion protein
Fragment
B
Females
Males
C
IFY-1:: GFPF
D
mSCF::LIN-41
lon-3(e2175)
lon-3 sel-10(ar41)
wild type
etc-1(gk5182)
sel-10(ok1632)
E
DNDF:: LIN-41
mSCF:: LIN-41
GFPF:: LIN-41